SYNTHESIS AND CHARACTERIZATION OF NOVEL MAX PHASE SOLID SOLUTIONS IN THE A SUBLATTICE

A Thesis

by

EVAN MILES PREHN

Submitted to the Office of Graduate and Professional Studies of
Texas A&M University
in partial fulfillment of the requirements for the degree of

MASTER OF SCIENCE

Chair of Committee,	Miladin Radovic
Committee Members,	Micah Green
	Xiaofeng Qian
Head of Department,	Ibrahim Karaman

May 2020

Major Subject: Materials Science and Engineering

ABSTRACT

MAX phases are a rapidly expanding family of atomically-layered carbides and nitrides known for their characteristically high temperature stability, excellent thermal shock resistance, good mechanical properties, and easy machinability. Approximately 70 pure MAX phases of different compositions and fewer than 100 solid solution alloys on M, A, or X sublattices have been successfully synthesized and characterized thus far. MAX phase solid solutions have gained particular interest recently as alloying of MAX phases facilitates tailoring of properties to particular applications and behaviors, yet the number of synthesized solid solutions is alarmingly small.

This work reports the first successful dedicated syntheses of new solid solutions of Ti_2AlC with bismuth and antimony, showing that maximum solubility of Bi and Sb on A sites are approximately 40at% and 70at%, respectively, and that substitution of Al with larger elements such as Bi and Sb leads to anisotropic stretching of the crystal cells. In this study, bulk, dense, predominantly phase-pure samples $Ti_2(Al_{1-x}Bi_x)C$ with x ranging from 0 to 0.4 were synthesized under argon at 1400˚C via Pulsed Electric Current Sintering from elemental powders. Maximum solubility of Bi in Ti_2AlC was found to be around 40% ($x = 0.4$), since all attempts to synthesize $Ti_2(Al_{1-x}Bi_x)C$ with $x > 0.4$ resulted in the phase decomposition of $Ti_2(Al_{1-x}Bi_x)C$. Substitution results in the formation of vacancies on Al-site and anisotropic stretching of the *a* lattice parameter from 3.06Å for $x = 0$ to 3.11Å for $x = 0.4$ with little effect on the *c* lattice parameter, as corroborated by X-Ray Diffraction and High-Resolution Scanning Transmission Electron

Microscopy. Increase in bismuth concentration results in an hardening of bulk $Ti_2(Al_{1-x}Bi_x)C$ phase without altering the elastic moduli.

Aluminum is also substituted with Sb in Ti_2AlC MAX up 70at%, observed in bulk, dense, phase-pure samples synthesized via Pulsed Electric Current Sintering. Incorporation of antimony results in anisotropic stretching of the *a* lattice parameter from 3.06Å to 3.13Å with corresponding shrinking of the *c* lattice parameter from 13.67Å to 13.53Å. In contrast with other large A element substitution (i.e. bismuth), antimony exhibits large thermodynamic preference toward formation of Ti_2Sb, resulting in more $Ti_3(Al_{1-x}Sb_x)C_2$ formed.

CONTRIBUTORS AND FUNDING SOURCES

Contributors

This work was supervised by a thesis committee consisting of Professor Miladin Radovic [advisor] and Professor Xiaofeng Qian of the Department of Materials Science and Engineering and Professor Micah Green of the Department of Chemical Engineering.

The computational results discussed in Section 2.2 were provided by Doctor Thien Duong. The HR-TEM analyses depicted in Section 2.2 were conducted by Doctor Jun Lu of the Department of Physics, Chemistry and Biology at Linköping University, Switzerland.

All other work conducted for the thesis was completed by the student independently.

Funding Sources

Graduate study was supported by the Engineering Graduate Merit Fellowship in the Department of Materials Science and Engineering at Texas A&M University and a Graduate Research Assistantship under Professor Miladin Radovic.

This work was also made possible in part by the National Science Foundation under Grant Numbers 1410983, 1729305, 1729335, and DGE-1545403. Its contents are solely the responsibility of the authors and do not necessarily represent the official views of the NSF.

TABLE OF CONTENTS

Page

ABSTRACT ii

CONTRIBUTORS AND FUNDING SOURCES iv

TABLE OF CONTENTS v

LIST OF FIGURES vi

LIST OF TABLES vii

CHAPTER I INTRODUCTION 1

CHAPTER II SYNTHESIS OF $Ti_2(Al_{1-x}Bi_x)C$ 7

Materials and Methods 7
Results and Discussion 11
Summary of Results 28

CHAPTER III SYNTHESIS OF $Ti_2(Al_{1-x}Sb_x)C$ 29

Materials and Methods 29
Results and Discussion 32
Summary of Results 39

CHAPTER IV SUMMARY 40

Closing Remarks 40
Conclusions 41
Implications and Future Work 42

REFERENCES 44

APPENDIX NOMENCLATURE 49

LIST OF FIGURES

Page

Figure 1 Common Crystal Structures of MAX Phases and Elements Forming Pure MAX Phases 2

Figure 2 Estimated Mixing Enthalpies of Ti_2AlC MAX Phases at 0K 3

Figure 3 Change of Temperature and Sample Thickness during Reaction Sintering of $Ti_2(Al_{1-x}Bi_x)C$ with Different Targeted Compositions 11

Figure 4 X-Ray Diffractograms of $Ti_2(Al_{1-x}Bi_x)C$ by Targeted Compositions 13

Figure 5 Selected but Typical Elemental EDS Map of $Ti_2(Al_{1-x}Bi_x)C$ for Targeted Composition x = 0.15 14

Figure 6 Representative Backscatter Electron Micrographs of $Ti_2(Al_{1-x}Bi_x)C$ for Different Targeted Amount of Bismuth, $0.00 \leq x \leq 0.80$ 15

Figure 7 Phase Compositions by Volume Percent of $Ti_2(Al_{1-x}Bi_x)C$ Samples for Different Targeted Compositions 16

Figure 8 (Al+Bi)/Ti Ratio in Mixed Powders and Bulk Sample as Determined Using Areal EDS Analysis 17

Figure 9 Amount of Bi, x, for $Ti_2(Al_{1-x}Bi_x)C$ Bulk Samples as Determined Using Areal EDS Analysis 19

Figure 10 $(Al_{1-x}Bi_x)$:2Ti Ratio, i.e. y in $Ti_2(Al_{1-x}Bi_x)_yC$ phase, in Powder Mixture and 211 Phases 20

Figure 11 Ordered $Ti_2(Al_{2/3}Bi_{1/3})C$ Structure with Al and Bi Alternatively Distributed at the Corner of an Al-Layer Hexagon of a 3 x 3 x 1 (72 atoms) Supercell 22

Figure 12 HRSTEM with SAED and EDS Results for $Ti_2(Al_{1-x}Bi_x)C$ with Targeted x = 0.20 and Targeted x = 0.30 24

Figure 13 HRSTEM with SAED and EDS Results for $Ti_2(Al_{1-x}Bi_x)C$ with Targeted x = 0.60 25

Figure 14 Sampling of *a* and *c* Lattice Parameters of $Ti_2(Al_{1-x}Bi_x)C$ 26

Figure 15 Vickers Hardness and Young's Modulus of $Ti_2(Al_{1-x}Bi_x)C$ Samples with Targeted Amounts of Bismuth Ranging from x = 0.00 to x = 0.30 26

Figure 16 X-Ray Diffractograms of $Ti_2(Al_{1-x}Sb_x)C$ for Observed Composition Ranging from x = 0.00 to x = 0.70 34

Figure 17 Selected *a* and *c* Lattice Parameters of $Ti_2(Al_{1-x}Sb_x)C$ 35

Figure 18 Phase Composition by Volume Percent for $Ti_2(Al_{1-x}Sb_x)C$ with Targeted Sb Amount Ranging from x = 0.00 to x = 0.70 as Determined by Rietveld Refinement of XRD Data 36

Figure 19 SEM and EDS data of $Ti_2(Al_{1-x}Sb_x)C$. 37

LIST OF TABLES

Page

Table 1 Summary of Some of the $Ti_2(Al_{1-x}Bi_x)C$ Phases Synthesized in This Study 8

Table 2 Vacancy Formation Energies Calculated for the Cases of Ordered-$Ti_2(Al_{2/3}Bi_{1/3})C$ and Disordered-$Ti_2(Al_{0.75}Bi_{0.25})C$ 23

Table 3 Summary of Some of the $Ti_2(Al_{1-x}Sb_x)C$ Phases Synthesized in This Study 31

CHAPTER I

INTRODUCTION

Ternary carbides and nitrides with the chemical formula $M_{n+1}AX_n$, where M is a transition metal, A is a late or post-transition metal, and X is carbon or nitrogen, commonly known as MAX phases, are a rapidly expanding family of atomically layered structures [1, 2, 3, 4]. Though the first MAX phase was synthesized in the early 1970s [3, 5, 6], little progress was made in characterizing this unique family of materials until the work of Barsoum *et al.* in 1996, in which a unique combination of properties was first reported for Ti_3SiC_2 as one of MAX phases [7]. MAX phase compounds are now known for their characteristically high temperature stability, excellent thermal shock resistance, good mechanical properties, and easy machinability [3]. Similar to binary carbides, MAX phases are characteristically excellent thermal and electrical conductors [8]. Some of them, predominantly those containing aluminum are also good candidates for high temperature applications as they exhibit remarkable oxidation resistance and crack-healing due to the formation of a protective Al_2O_3 shell [9, 10].

Approximately 70 pure MAX phases of different compositions and around 100 solid solution alloys on M, A, or X sublattices have been successfully synthesized and characterized to date [4] **Figure 1**. The latter group has gained particular interest recently as alloying of MAX phases facilitates tailoring of properties to particular applications. Substitution in one or more of the sub-lattices facilitates discreet, independent fine-tuning of the metallic and ceramic traits of MAX phases; indeed, MAX phase alloying is vital to expanding the MAX phase compositional space, as several elements on the M-site and A-site are stable in solution but do not form pure MAX phases [11, 12, 13]. Further, alloying on the M sublattice allows for in-plane and out-of-

plane ordering of the alloyed element, known as i-MAX and o-MAX, respectively [14, 15, 16, 17]. These ordered structures are particularly exciting as they facilitate the production of novel 2D derivative of MAX phases commonly referred to as MXenes, with ordered vacancies [18, 19].

(a)

(b)

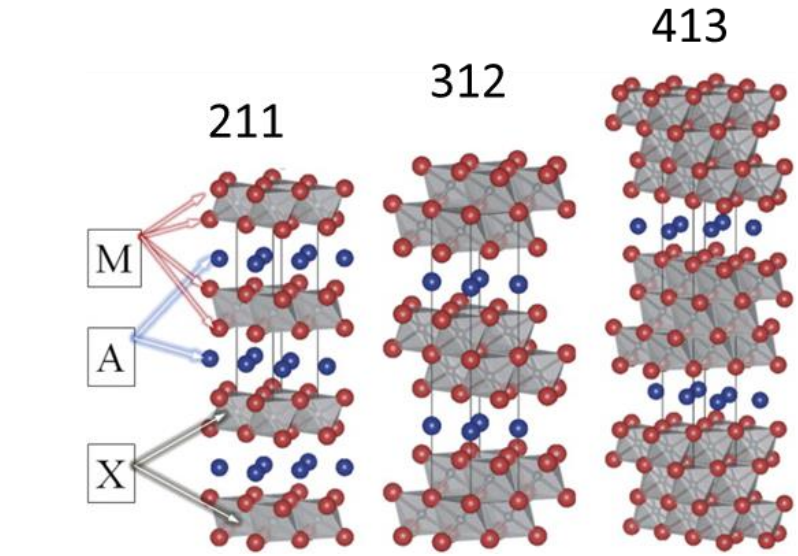

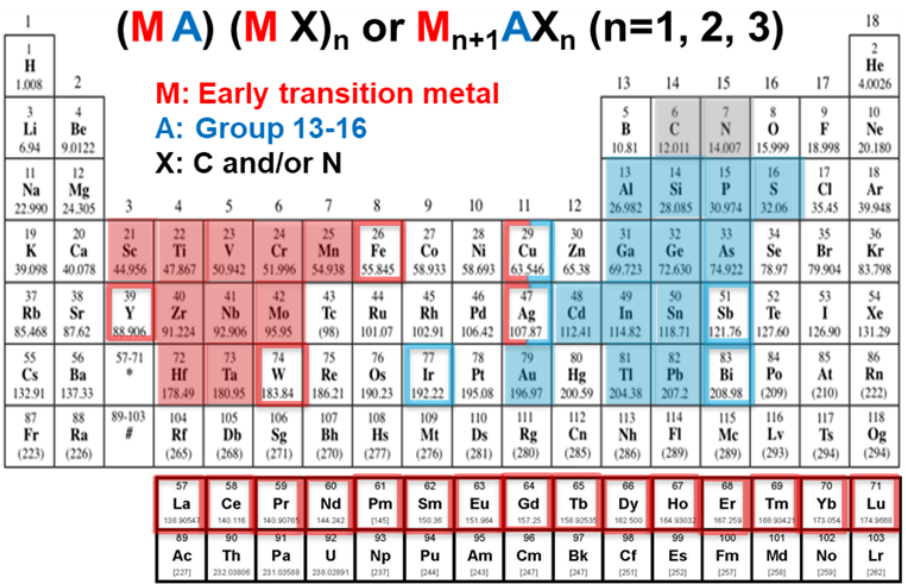

Figure 1. (a) common crystal structures of MAX phases (b) elements forming pure MAX phases (M-solid red, A – solid blue, X – solid gray). Elements that can only form solid solutions are enclosed in the frame (M-red frame, A-blue frame). Reprinted from [4].

Despite this growing interest in tailoring properties of MAX phases by their alloying on M, A or X site, only a small portion of a practically indefinite number of possible MAX phase solid solutions have been synthesized and characterized to date [20]. Most alloying work has focused on the M-sublattice, combining elements that normally form MAX phases such as Ti, V, Cr, etc., or incorporating elements that do not form pure MAX phases such as yttrium, manganese, iron, rare earths, etc. [17, 21, 22]. Surprisingly, the previous work on solid solutions in the A-sublattice is even more limited and typically focus on smaller elements such as aluminum, silicon, and gallium [23, 24]. The only exceptions include attempts to substitute Al in Ti_3AlC_2 with much larger Sn (x) and works of Horlait *et al* [10, 12] *and* Lapauw *et al* [25] probing of Zr_2AlC with much larger elements such as Sn, Sb, and Pb to stabilize these MAX phases.

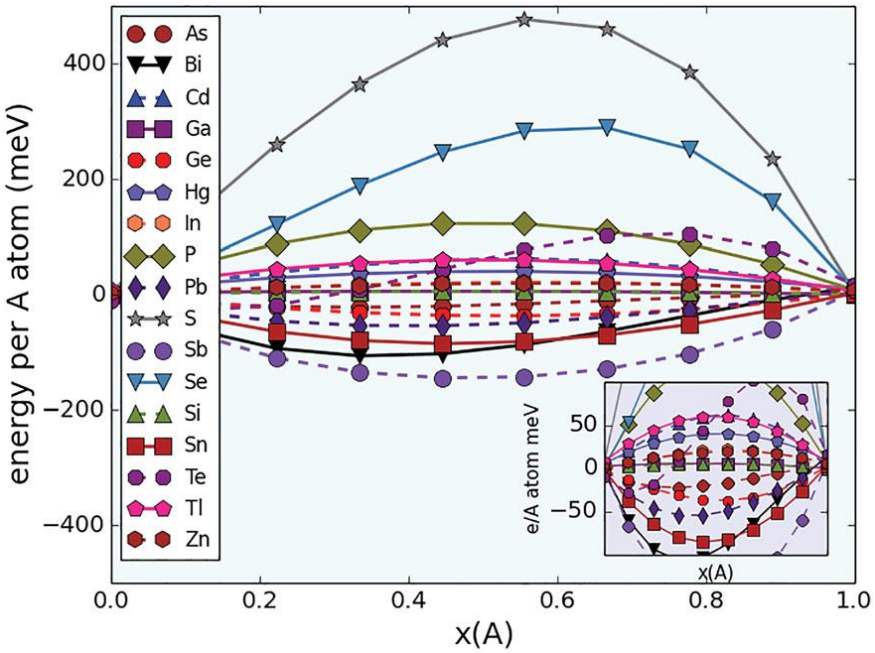

Figure 2. Estimated mixing enthalpies of Ti_2AlC MAX phases at 0K. The results indicate $Ti_2(Al,Bi)C$ is one promising MAX solution. Reprinted from [23].

In a recent study Arróyave *et al.* used cluster expansion to systematically explore the stability of Ti_2AlC, Ti_3AlC_2, and Zr_3AlC_2 alloyed with different A-site elements from groups 12-16, ***Figure 2*** [23]. Results of this study suggest that the M-element (Ti or Zr) and stacking of MAX phase (e.g. 211 vs. 312) plays a relatively small role in the stability of A-sublattice alloys. Interestingly enough, although substitution of Al in those MAX phases with much larger elements from groups 14 and 15, namely Ge, Sb, Bi, Sn, and Pb, should result in the formation of stable MAX phase solid solutions, only one of them, $Ti_2(Al_{1-x}Sn_x)C$, has been studied with any rigor [24, 26, 27]. Additionally, it is worth noting that while Ge, Pb, and Sn form pure "end-member" MAX phases (Ti_2GeC, Ti_2PbC, Ti_2ZnC and Ti_2SnC, respectively) [28, 29, 30], no pure MAX phases have been synthesized using Sb or Bi until now. Interestingly, each of these A-site alloys is in direct violation of the first Hume-Rothery rule since the atomic radius of bismuth is nearly 22% larger than that of aluminum.

The only bismuth-containing MAX phase synthesized to date is $Zr_2(Al_{1-x}Bi_x)C$ [10]. This finding further supports the validity and utility of the aforementioned work by Arróyave *et al.* [23], namely the stability of bismuth-containing MAX phases. However, this work did not establish the maximum solubility of bismuth into an aluminum A layer, instead focusing on a single experimentally-observed stoichiometry of $Zr_2(Al_{0.42}Bi_{0.58})C$. In this study Horlait et al. [10, 12] originally predicted increases in both the *a* and *c* lattice parameters with increasing x for $Zr_2(Al_{1-x}Bi_x)C$; however, later computational work on this system indicates an increase in *a* lattice parameter with inconsistent *c* distortions [10, 12, 30]. Such stretching is unusual given the large unit cell [32]. More importantly, Horlait *et al.* [10, 12] synthesized the first Bi containing MAX phase by substituting Al with much larger Bi in Zr_2AlC, i.e. the parent phase with much large

lattice parameters (a = 3.33 Å, c = 14.57 Å), when compared to more commonly used MAX phases such as Ti_2AlC (a = 3.04 Å, and c = 13.60 Å) [2]. Indeed, the comparatively small lattice of Ti_2AlC must undergo much more significant distortion to accommodate the large element substitution, as evidenced by the work of Greil *et al.* on $Ti_2(Al_{1-x}Sn_x)C$ [24]. As tin is substituted into aluminum in the aforementioned work, the c/a ratio decreases linearly due to "significant expansion along the a axis . . . [while] c remains almost constant" [24].

The only antimony-containing MAX phase synthesized to date is $Zr_2(Al_{1-x}Sb_x)C$, [10] again supporting predictions by Arróyave *et al.* [23], showing that Sb can form a stable solid solution on both Ti and Zr based MAX phases. However, as in the case of solid solutions with Bi, this work [10] did not establish the maximum solubility of antimony into an aluminum A layer, instead focusing on a single experimentally-observed stoichiometry: $Zr_2(Al_{.30}Sb_{.70})C$. Also, as Ti_2AlC has much smaller lattice parameters than Zr_2AlC, substitution of Al in Ti_2AlC with much larger Sb is more challenging, as it requires larger lattice distortions.

Tailoring of MAX phase lattice parameters via A-site alloying, especially with atoms having much larger atomic radius, has many ramifications in both academic and industrial realms, including facilitating easier intercalation between the sublattices for energy storage applications. Another specific, industrial consequence of large-element substitution is in the production of MXenes. These 2D materials are created by removing the A-layer element, typically via chemical etching [17]. The most challenging step in MXene etching is the intercalation of the etchant between M-layers, which affects the yield purity, processing time, and degree of delamination [17]. Substitution of large constituents in the A-layer should result in better

intercalation, which may lead to previously unobtainable MXenes. Other implications of this work for general MAX phases include (a) improved efficacy in nuclear and x-ray cladding (by increasing bulk density), (b) improved thermal fatigue resistance (by compensating for thermal expansion of other constituents), and (c) improved safety in processing antibacterial $Ti_3C_2T_x$ MXenes [17, 25, 33].

This work intends to elucidate the possibilities of A-element substitution in MAX phases, specifically Ti_2AlC, with much larger elements such as bismuth (Bi) and antimony (Sb) to:

(i) To validate the cluster-expansion predictions by Arróyave *et al.* that both Sn and Bi can form stable solid solutions on A-site in Ti_2AlC;

(ii) Establish the solubility limits of bismuth and antimony on the A-layer ion Ti_2AlC MAX phase; and

(iii) Characterize the effects of Sn and Bi substitution on A-sublattice on the lattice parameters of T_2AlC.

CHAPTER II

SYNTHESIS OF $Ti_2(Al_{1-x}Bi_x)C$

Materials and Methods

Titanium, bismuth, aluminum, and graphite elemental powders (all from Alfa Aesar, MA) were mixed with a Ti:Al:Bi:C stoichiometry of 2 : 1.2(1-x) : 1.25(x) : 0.95. Additional amounts of low-melting point Al and Bi were added to compensate for their leakage and volatilization during pressure assisted reactions sintering to MAX phase. Exact mixing ratios of elemental powders for different $Ti_2(Al_{1-x}Bi_x)C$ solid solutions synthesized in this study are provided in **Table 1**. Note that the powder mixing rations presented in **Table 1** are selected after trying several different mixing ratios (not shown here) for each targeted composition, as those mixing ratios resulted in samples with the highest fraction of 211 MAX phase. The powders were mixed for 6 hours via ball-milling, then packed into a 20 mm graphite die and reaction sintered using a Pulsed Electric Current Sintering System (Thermal Technologies LLC, CA). Samples were heated to 800°C at a rate of 25°C/min to allow molten bismuth to be dissolved into aluminum. After 5 minutes, the pressure on the samples was increased to 15 MPa at a rate of 10 MPa/min and resumed heating at a rate of 25°C/min up to 1400°C. The temperature and pressure were held constant for 15 minutes before rapid cooling and pressure relief. To test for possible A-site degradation due to rapid heating and cooling, selected powder compositions with identical stoichiometries were placed in alumina boats and heated in a MTI Corporation high-vacuum tube furnace under argon atmosphere. Samples were heated at a rate of 10°C/min to 1400°C, the observed formation temperature of Al-Bi intermetallics, and held for 1 hour. Reacted powders were cooled to room temperature under Argon then grinded and sintered using an SPS system at the above conditions.

Table 1. Summary of some of the $Ti_2(Al_{1-x}Bi_x)C$ phases synthesized in this study. Included are mixing ratios of initial powders, and results of XRD, SEM and EDS analysis.

	Powder mixing ratio		**XRD results**		**SEM and EDS results**				
Target x	**Ti : (Al+Bi) : C**	**Al : Bi**	**Lattice Parameters (Å)**	**Results of Rietveld analysis**	**% of MAX phases from ImageJ**	**x for entire sample**	**(Al+Bi) /Ti Ratio**	**x in 211 MAX phase**	**Actual Stoichiometry (assuming C≈1.0)**
x = 0.00	2.0 : 1.150 : 0.95	1.15 : 0.00	*a* = 3.06 *c* = 13.67	81% 211 + some 312 and $TiAl_3$	96.39	-	0.48	-	$\mathbf{Ti}_2Al_{0.96}$
x = 0.10	2.0 : 1.205 : 0.95	1.08 : 0.125	*a* = 3.08 *c* = 13.67	95% 211 + some TiC and $TiAl_3$	97.74	x = 0.12	0.49	0.12±0.005	$\mathbf{Ti}_2(Al_{0.88}Bi_{.12})_{0.95}$
x = 0.20	2.0 : 1.210 : 0.95	0.96 : 0.25	*a* = 3.08 *c* = 13.67	94% 211 + some 312 and $TiAl_3$	96.65	x = 0.16	0.51	0.17±0.005	$\mathbf{Ti}_2(Al_{0.83}Bi_{.17})_{1.00}$
x = 0.30	2.0 : 1.215 : 0.95	0.84 : 0.37	*a* = 3.10 *c* = 13.65	93% 211 + some TiC and $TiAl_3$	96.86	x = 0.18	0.47	0.27±0.005	$\mathbf{Ti}_2(Al_{0.73}Bi_{.27})_{0.97}$
x = 0.40	2.0 : 1.220 : 0.95	0.72 : 0.50	*a* = 3.10 c = 13.69	95% 211 + some TiC and $TiAl_3$	93.58	x = 0.20	0.44	0.20±0.002	$\mathbf{Ti}_2(Al_{0.80}Bi_{.20})_{0.94}$
x = 0.50	2.0 : 1.225 : 0.95	0.60 : 0.62	*a* = 3.11 *c* = 13.68	96% 211 + some TiC and $TiAl_3$	88.54	x = 0.28	0.40	0.28±0.004	$\mathbf{Ti}_2(Al_{0.72}Bi_{0.28})_{0.93}$
x = 0.60	2.0 : 1.230 : 0.95	0.48 : 0.75	*a* = 3.11 *c* = 13.68	81% 211 + some TiC	84.24	x = 0.32	0.34	0.31±0.003	$\mathbf{Ti}_2(Al_{0.69}Bi_{.31})_{0.93}$
x = 0.80	2.0 : 1.240 : 0.95	0.24 : 1.00	*a* = 2.89 *c* = 13.63	81% 211 + some TiC	64.43	x = 0.42	0.22	0.38±0.002	$\mathbf{Ti}_2(Al_{0.62}Bi_{.38})_{0.91}$

The surfaces of resulting bulk samples were manually polished and examined using X-Ray diffraction (XRD, D8-Focus Bragg-Brentano X-ray Powder Diffractometer, Bruker). The resulting diffractograms were examined using DIFFRAC.EVA (Bruker) and TOPAS (Bruker) software. Presence and intensity of the characteristic 211 MAX phase peak at $2\Theta \approx 13°$ was used to quickly determine the presence of the targeted MAX phase. Le Bail refinement was performed to determine the lattice parameters of the primary phases, and Rietveld refinement was used to quantify the phase ratios (by volume) in the bulk. All peak labels and crystal structure information were obtained from the Inorganic Crystal Structure Database (ICSD), and the background was modeled as an amorphous *hkl* phase. Lattice parameters for Rietveld refinement were taken from the results of the Le Bail refinement, and a maximum allowable error threshold was set to $R_{wp} \approx 9.0$.

Reaction sintered samples were cut after XRD analysis with a water-cooled low-speed, mounted in epoxy resin (EpoxiCure^{TM}, Buehler), and mechanically polished up to 0.1 µm diamond suspension for Scanning Electron Microcopy (SEM, JEOL 7500). Surface morphology of samples was characterized via an Everhart-Thornley detector (ETD), while sample phase purity was characterized by a low-angle backscatter electron (LABE) detector. Phase composition was estimated from back-scatter electron images using ImageJ software. An energy dispersion X-ray spectroscopy (EDS) detector, which was operated via INCA (Oxford Instruments) software, was used to obtain chemical composition of the primary, 211 MAX phases as well as other impurities presented in the samples. For each sample, a composition was collected using EDS at a minimum of 60 data points.

The atomic structure analysis of select samples was carried out by High–Resolution Scanning Transmission Microscope (HR-STEM) double Cs-corrected FEI Titan3 60−300 operated at 300 kV, equipped with a Super-X EDX system, in collaboration with Linköping University, Sweden. The chemical composition of the samples was also measured by energy-dispersive X-ray (EDX) analysis in a Leo 1550 Gemini with Oxford INCA EDX. Selected area electron diffraction (SAED) characterization was carried out using a FEI Tecnai G2 TF20 UT instrument operated at 200 kV. Transmission electron microscopy (TEM) powder specimens were prepared by dispersing a small amount of powder sample onto a carbon film grid.

Hardness was measured with a Vickers Hardness indenter (LECO Corporation) using a force of 1 kN in at least 10 different locations at each sample with differed composition. Elastic properties were measured via Resonant Ultrasound Spectroscopy (RUS) using procedures described in more detail elsewhere [34, 35, 36, 37], for each sample excepting $Ti_2(Al_{0.62}Bi_{.38})_{0.91}C$, in which brittle impurities skewed the results.

Results and Discussion

Selected but typical sintering curves for $Ti_2(Al_{1-x}Bi_x)C$ with different targeted compositions are shown in **Figure 3**. After initial expansion of the powder mixture during heating, a sudden drop in the piston position can be observed at around 270ºC due to the melting of the Bi. From that point, reaction of molten Bi with solid Al to form higher melting point Al-Bi alloys is the reason for

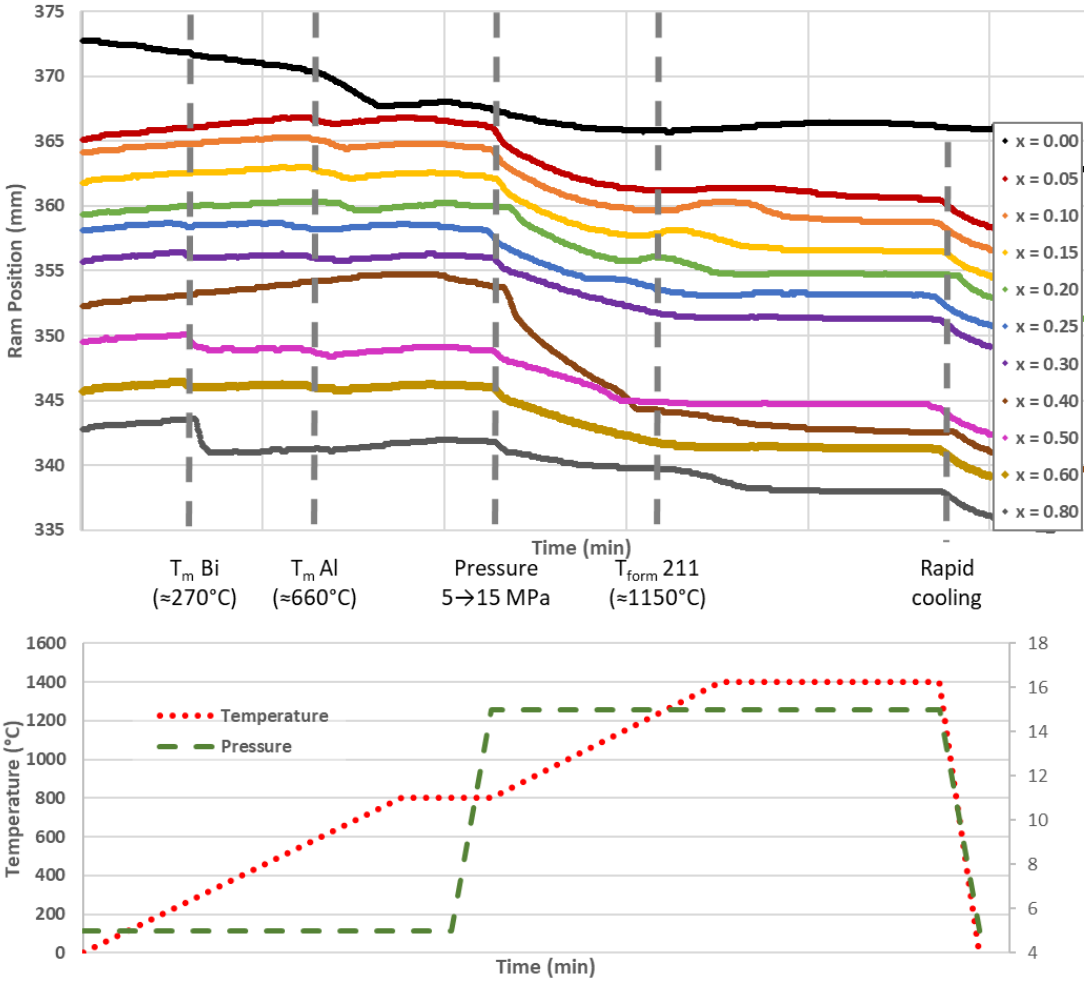

Figure 3. Change of temperature and sample thickness (sintering curves) during reaction sintering of $Ti_2(Al_{1-x}Bi_x)C$ with different targeted compositions.

further sample expansion until aluminum melts at around 660^{o}C. Formation of those two melts is the reason for carrying out initial reaction sintering under very low pressure of 5 MPa, which is high enough to secure good contact of pistons with the sample during sintering but minimizes leakage of the molten products. At around 800^{o}C when majority of the molten Al-Bi products react with Ti, the pressure was increased to 15 MPa, as indicated by the significant compaction of the samples at around 1150^{o}C. Most of the reaction sintering seems to be almost completed by the time the sintering temperature reaches 1400^{o}C since no significant changes in the sample thickness can be observed during soaking at 1400^{o}C.

Figure 4 shows the XRD results for each $Ti_2(Al_{1-x}Bi_x)C$ sample as a function of *x*, where *x* is the percent of targeted bismuth percent as listed in ***Table 1***. Those results, as well as results of Rietveld analysis in **Table 1**, clearly show that the majority phase in all samples is $Ti_2(Al_{1-x}Bi_x)C$, with small amounts of $Ti_3(Al_{1-x}Bi_x)C_2$, TiC and $TiAl_x$ (mostly $TiAl_3$) intermetallic impurities. Note here that higher amounts of $Ti_3(Al_{1-x}Bi_x)C_2$ and $TiAl_3$ are detected in samples with targeted x = 0 (i.e. in Ti_2AlC) most likely because of the incomplete reaction at the selected sintering conditions. Later suggests that addition of small amount of Bi might be a good sintering aid for reaction SPSing of Ti_2AlC. More importantly, XRD results in **Figure 4** and **Table 1** clearly show that addition of Bi, especially for targeted composition x > 0.5, results in formation of the substantial amount of TiC as a secondary phase, suggesting excessive loss of Bi during sintering as a result of its melting and volatilization.

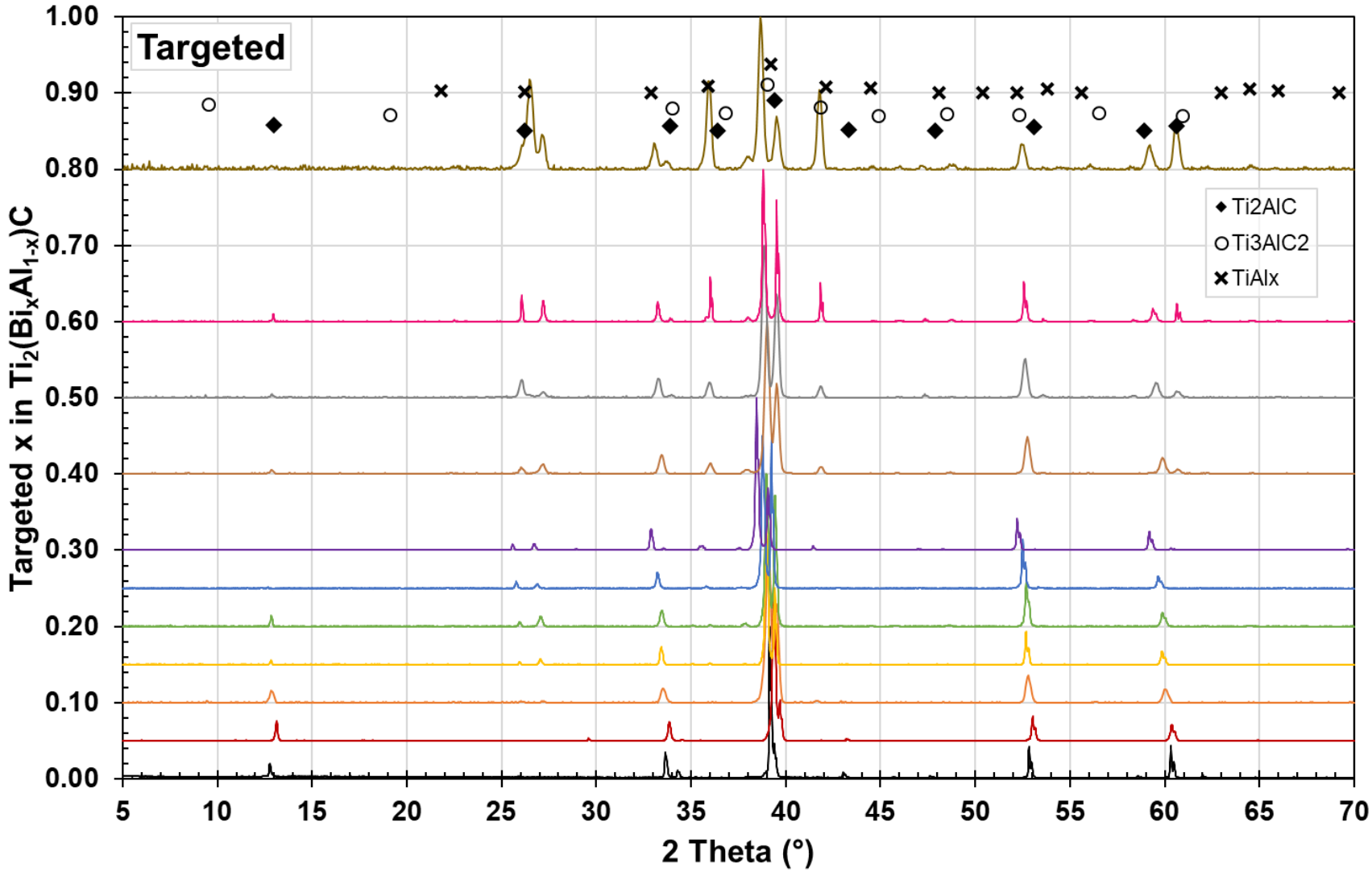

Figure 4. X-ray diffractograms of $Ti_2(Al_{1-x}Bi_x)C$ by targeted compositions.

SEM results in **Figures 5** and **6**, further confirm that all reaction sintered samples contains mostly of $Ti_2(Al_{1-x}Bi_x)C$ (or 211 phase) with some $Ti_3(Al_{1-x}Bi_x)C_2$ (or 312 phase), $TiAl_x$ and TiC impurities. Note here that all added Bi tends to form solid solution only with Ti_2AlC phase, but not with $TiAl_x$ impurities, as it is illustrated in **Figure 5**. Different phases labeled in **Figure 6** were identified based on their chemical composition using EDS (results not shown here), and the phase compositions for $Ti_2(Al_{1-x}Bi_x)C$ samples with different *x* were determined from SEM micrographs based on the phase contrast using ImageJ. Results of this analysis are further compared to results of Rietveld analysis in **Table 1** and **Figure 7** and they once again confirm that addition of the larger amount of Bi, especially for targeted compositions x > 0.5, results in the formation of substantial amount of TiC as a major impurity phase. When compared to Rietveld analysis, slightly higher amount of impurity phases was determined using ImageJ analysis for samples with x > 0.5, mostly because the size of some impurities is too small to be detected accurately using XRD analysis.

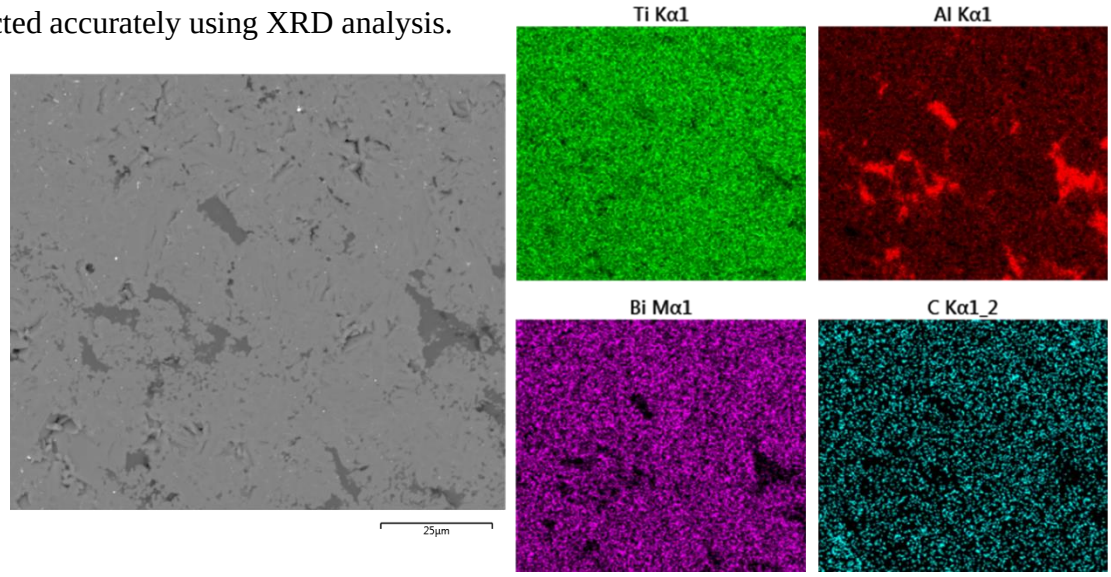

Figure 5. Selected but typical elemental EDS map of $Ti_2(Al_{1-x}Bi_x)C$ for targeted composition x = 0.15. Data shows bismuth substitution in 211 MAX phase but not in the $TiAl_x$ intermetallic impurities.

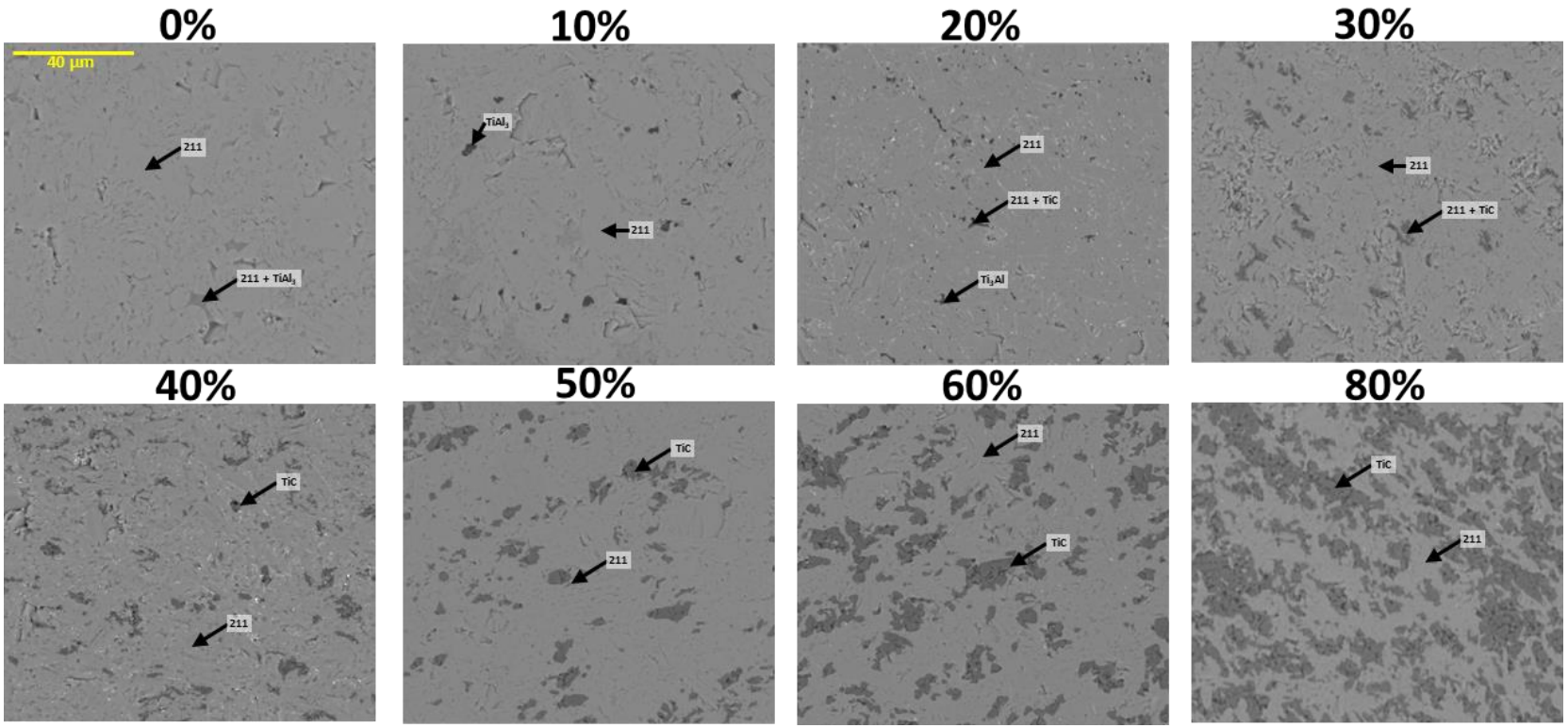

Figure 6. Representative Backscatter electron micrographs of $Ti_2(Al_{1-x}Bi_x)C$ for different targeted amount of bismuth, $0.00 \leq x \leq 0.80$ (contrast adjusted for consistency, taken at same magnification). Different phases were identified based on their composition determined using EDS (results not shown here).

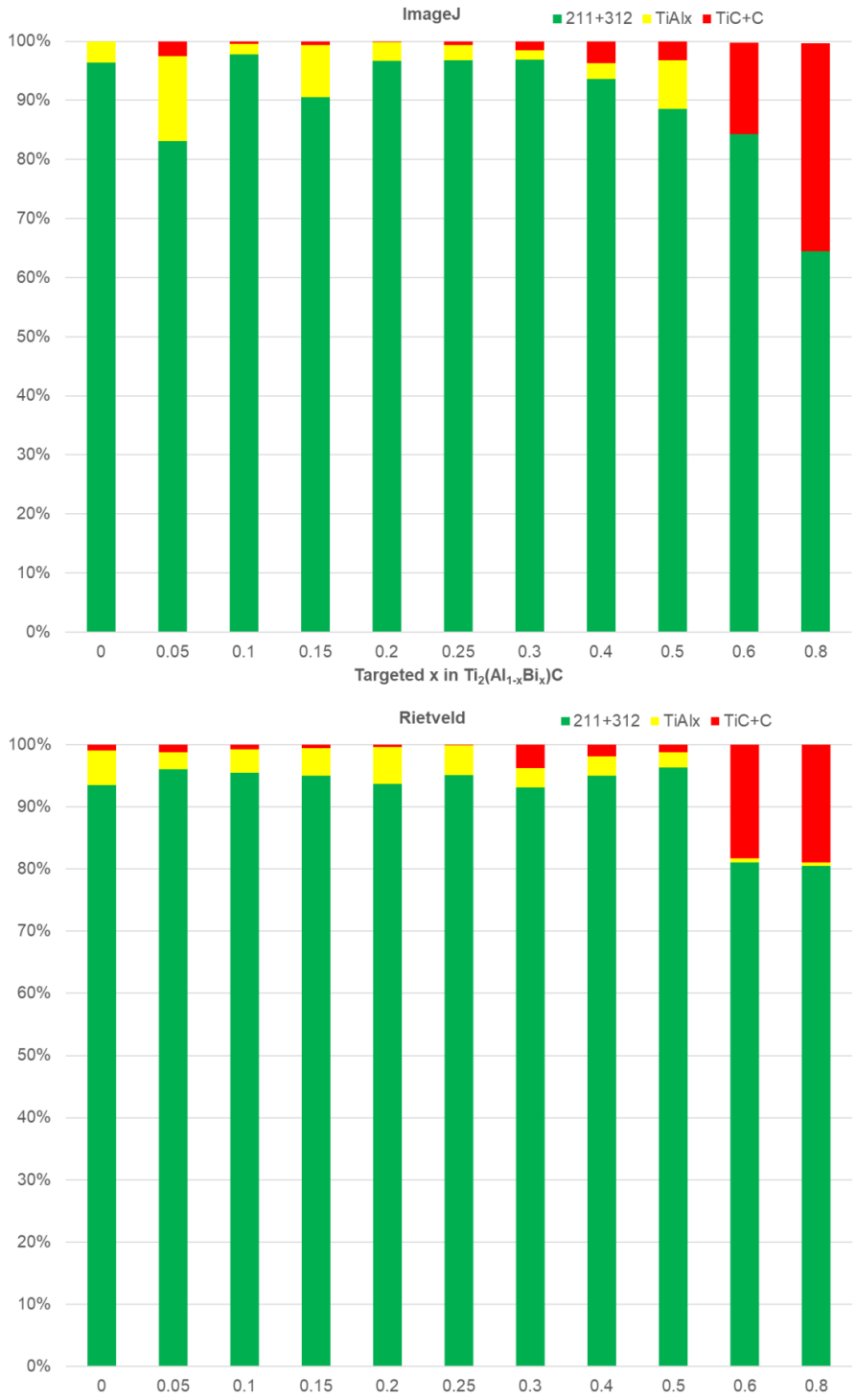

Figure 7. Phase compositions by volume percent of $Ti_2(Al_{1-x}Bi_x)C$ samples for different targeted compositions. Targeted compositions varied $0.00 \leq x \leq 0.80$, and purities calculated by (a) image analysis of representative Backscatter electron SEM micrographs such as those shown in Figures 5 and 6, and (b) Rietveld refinement of XRD data shown in Figure 4.

The fact that amount of unreacted TiC increases with increasing Bi content **(Table 1, Figures 4-7)**, with almost constant, but very small amount of $TiAl_X$ impurity that does not contain any detectible level of Bi, strongly suggests the amount of low melting point Bi in the reaction sintered samples is well below targeted amount *x*, due to its melting and volatilization at relatively low temperatures (**Figure 3**). Therefore, quantitative EDS analysis was carried out for each sample with different *x* to (i) determine chemical composition of the entire sample by analyzing overall composition of the ~100x150 µm representative area and (ii) determine composition of major $Ti_2(Al_{1-x}Bi_x)C$ (i.e. 211) phase in at least 10 points. The results of this analysis are summarized in **Table 1** and **Figures 8-10**.

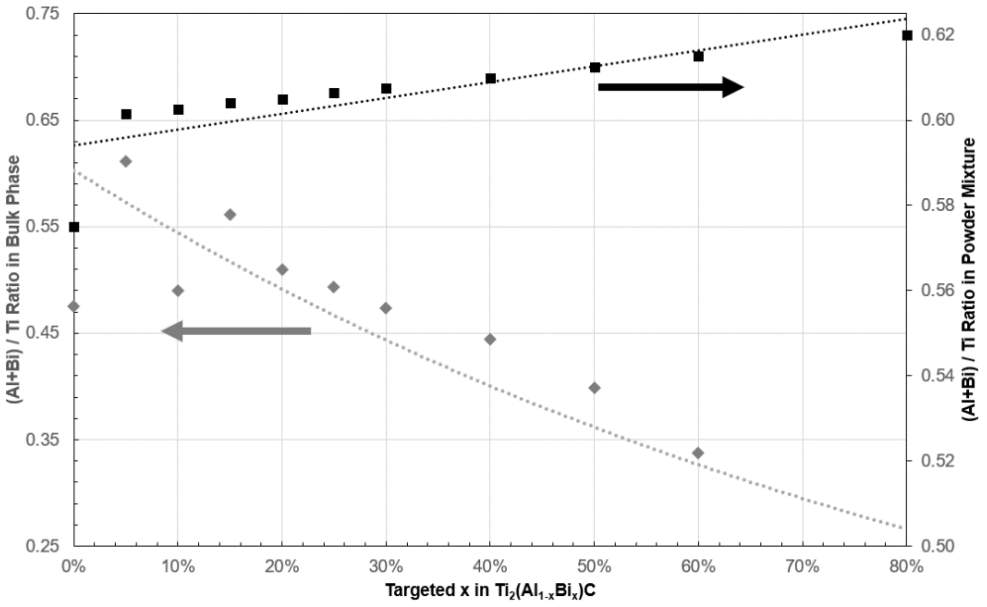

Figure 8. (Al+Bi)/Ti ratio in mixed powders and bulk sample as determined using areal EDS analysis. Samples shown by different targeted amount of Bi, x.

Figure 8 clearly shows that the amount of (Al+Bi)/Ti ratio as determined using areal EDS analysis for samples with different targeted Bi amount, *x*, decreases continuously with increasing

amount of *x*, regardless of the fact that the larger amount of A elements was added to the initial powder mixture to compensate for extensive leaking and volatilization of primarily low melting Bi. However, results plotted in **Figure 9** suggests that all most of the Bi that remains in the sample after sintering is actually dissolved in $Ti_2(Al_{1-x}Bi_x)C$ solid solution, because *x* calculated from the areal EDS analysis are almost identical to that determined using EDS point analysis in 211 phase. The only exception is sample with targeted composition of x = 0.3, where the amount of bismuth in 211 phase is significantly higher than in the equilibrium intermetallics. One possible explanation for this phenomenon is a local energy well based on lattice stretching and vacancies, allowing bismuth and aluminum to "fit" together preferentially at a ratio of 0.33 : 0.66. Based on the EDS point analysis in 211 phase, the stoichiometries of the 211 phases in samples with different targeted compositions were determined and are listed in the last column of **Table 1**. These results are in good agreement with EDS maps illustrated in **Figure 5**, showing that Bi is mostly contained in 211 phase and not in the $TiAl_x$ intermetallic. Therefore, because the amount of $TiAl_x$ impurities is relatively small, difference between x values determined from the areal EDS and point EDS analysis in 211 phase should be minimal (excepting x = 0.30), as shown in **Figure 9**.

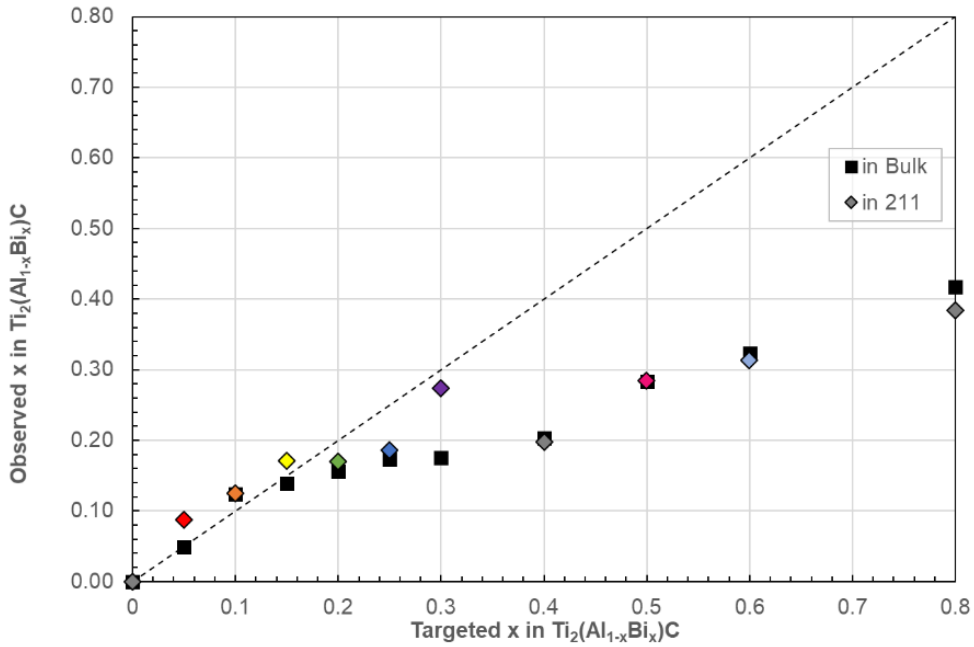

Figure 9. Amount of Bi, x, for $Ti_2(Al_{1-x}Bi_x)C$ bulk samples as determined using areal EDS analysis. Samples shown by different targeted amount of Bi, x.

Figure 9 also shows that the x determined in $Ti_2(Bi_xAl_{1-x})C$ samples have values almost identical to the targeted values for samples with targeted x below ~0.2. Above this targeted value, x determined in $Ti_2(Bi_xAl_{1-x})C$ deviates more from the targeted value, reaching the maximum value of ~0.4 for that sample with targeted x = 0.8. Since samples with higher targeted values also contain substantial amount of impurities, mostly TiC it is reasonable to conclude that x = 0.4 is close to the maximum solubility limit of Bi in Ti_2AlC that can be practically achieved under described sintering conditions. Further attempts to synthesize samples with targeted x = 0.9 (not shown here) resulted in complete phase decomposition of the samples and formation of predominantly TiC.

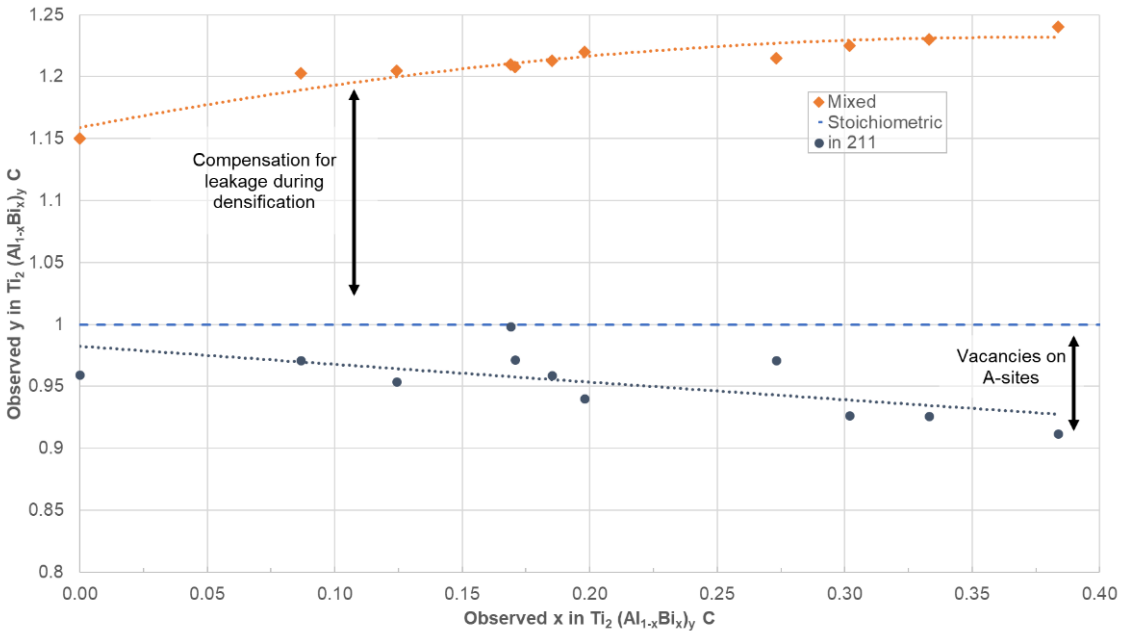

Figure 10. $(Al_{1-x}Bi_x)$:2Ti ratio, i.e. y in $Ti_2(Al_{1-x}Bi_x)_yC$ phase, in powder mixture and 211 phases. Analysis determined using point EDS for samples with different observed amount of Bi, x in 211 phase. Dashed blue line represent stoichiometric ratio expected for 211 phases.

To further analyze composition of 211 phase in the reaction sintered samples with different targeted compositions, $(Al_{1-x}Bi_x)$:2Ti ratio, i.e. y in $Ti_2(Al_{1-x}Bi_x)_yC$ phase determined using point EDS analysis is plotted in the function of the observed amount of Bi in the 211 phase, **Figure 10**. Note here that *y* in $Ti_2(Al_{1-x}Bi_x)_yC$ continuously decreases with increasing amounts of Bi in 211 phase, reaching a minimum value of around 0.92 for 211 phase with determined composition of $Ti_2(Al_{0.62}Bi_{.38})_{0.91}C$, i.e. with targeted Bi amount of x = 0.8. Results in **Figure 10** suggest that substitution of Al with significantly larger Bi results in formation of sub-stoichiometric $Ti_2(Al_{1-x}Bi_x)_yC$ phase with y < 1 due to the formation of vacancies on the A-sublattice to accommodate larger Bi atoms.

Further evidence for the formation of vacancies on A-sites as a result of substitution of Al in Ti_2AlC with Bi can be find in the computational study on the vacancy formation energies in this solid-solution system [38]. In this study, vacancy formation energies of $Ti_2(Al_{1-x}Bi_x)C$ were investigated assuming they form only on Al sites. The formation energies were calculated using the following formula:

$$E_f^{Al} = E_{Defect} - E_{Perf} + \mu_{Al}$$

where E_{Defect} is the energy of $Ti_2(Al_{1-x}Bi_x)C$ containing one Al-vacancy, E_{Perf} is the energy of a perfect $Ti_2(Al_{1-x}Bi_x)C$ with no vacancy, and μ_{Al} is the partial chemical potential of Al which is approximated by the energy of one atom of Al in the current work. Two cases were theoretically investigated:

I. Ordered $Ti_2(Al_{2/3}Bi_{1/3})C$, Al and Bi atoms are alternatively located at the corners of a hexagon on the Al-layer, as demonstrated in **Figure 11**. This configuration is believed to equally distribute strain raised by the size difference between Al and Bi atoms over the entire structure and as such minimize the total strain energy. To model the perfectly ordered structure, a supercell of $3 \times 3 \times 1$ (72 atoms) was used. For the defect structure, the vacancy is introduced at the Al-site located at the center of the hexagon.

II. Disordered $Ti_2(Al_{0.75}Bi_{0.25})C$: a 71-atom and 72-atom special quasi-random structures (SQS) were used to model the $Ti_2(Al_{1-x}Bi_x)C$ off-stoichiometric (partially disordered) alloys with and without vacancy, respectively. By using SQS to model the vacancy-

containing structure, the local effects of a vacancy on the chemistry of the alloys are observed, assuming for simplicity that only the configurational effect matters.

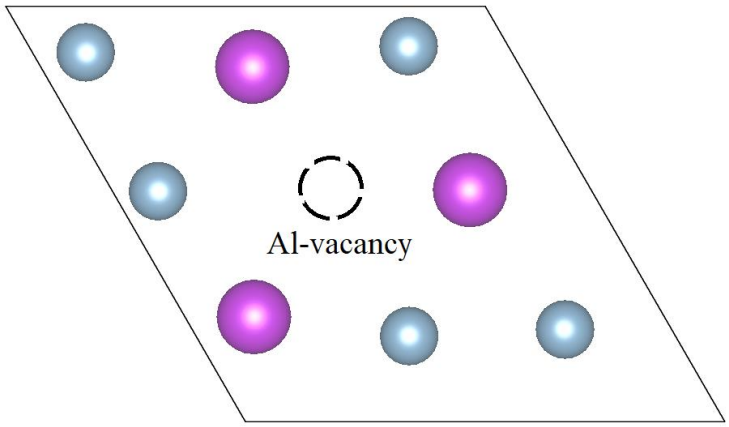

Figure 11. Ordered $Ti_2(Al_{2/3}Bi_{1/3})C$ structure with Al and Bi alternatively distributed at the corner of an Al-layer hexagon of a 3 x 3 x 1 (72 atoms) supercell.

The energies of the modeled structures were evaluated by first-principles calculations in that study [38]. The setups of these calculations are the same as those described above. The results of the first-principles calculations are shown in **Table 2**. It can be seen from this table that Al-vacancy is favored in the $Ti_2(Al_{1-x}Bi_x)C$ alloy (with negative vacancy formation energy!). In contrast to previous beliefs, the current first-principles calculations and experiments indicate that stable solid solutions can exist with stoichiometry departing significantly from that of typical MAX phases (> 5%). Interestingly enough, first-principles calculations also predict that $Ti_2(Al_{1-x}Bi_x)C$ has a slight tendency toward vacancy-driven ordering (i.e. the vacancy formation energy of ordered $Ti_2(Al_{2/3}Bi_{1/3})C$ is lower than that of the alloy at the same Al/Bi concentration).

Table 2. Vacancy formation energies calculated for the cases of ordered-$Ti_2(Al_{2/3}Bi_{1/3})C$ and disordered-$Ti_2(Al_{0.75}Bi_{0.25})C$.

Vacancy formation energy (eV) on A-site	
Ordered –$Ti_2(Al_{2/3}Bi_{1/3})C$	**Disordered-$Ti_2(Al_{0.75}Bi_{0.25})C$**
-2.07	**-1.55**

To further investigate possible ordering of Bi on A-sublattice $Ti_2(Al_{1-x}Bi_x)C$, selected solid solutions were investigated using HR-STEM, **Figures 11-13.** The HR-STEM results do not indicate any tendencies of Bi ordering on A-sublattice, even for the sample $Ti_2(Al_{0.69}Bi_{0.31})C$, which is close in the composition to the modeled one with stoichiometry of $Ti_2(Al_{0.69}Bi_{0.31})C$. This inconsistency is most likely due to the system remaining metastable after fast SPS processing, and closer inspection would require subsequent long heat-treatment to reach an equilibrium state (while avoiding volatilization of bismuth). Subsequent investigations are needed to resolve the disagreement between the experiments and calculations. However, results in **Figures 11-13** show a tendency of Bi clustering on A-sublattice even in samples having Bi content as low as 0.17. This further supports the theory that flash-reaction sintered $Ti_2(Al_{1-x}Bi_x)C$ are in metastable states. In addition, analysis of HR-STEM results shows that the *a* lattice parameter increases with increasing Bi content, while *c* lattice parameter remains almost constant.

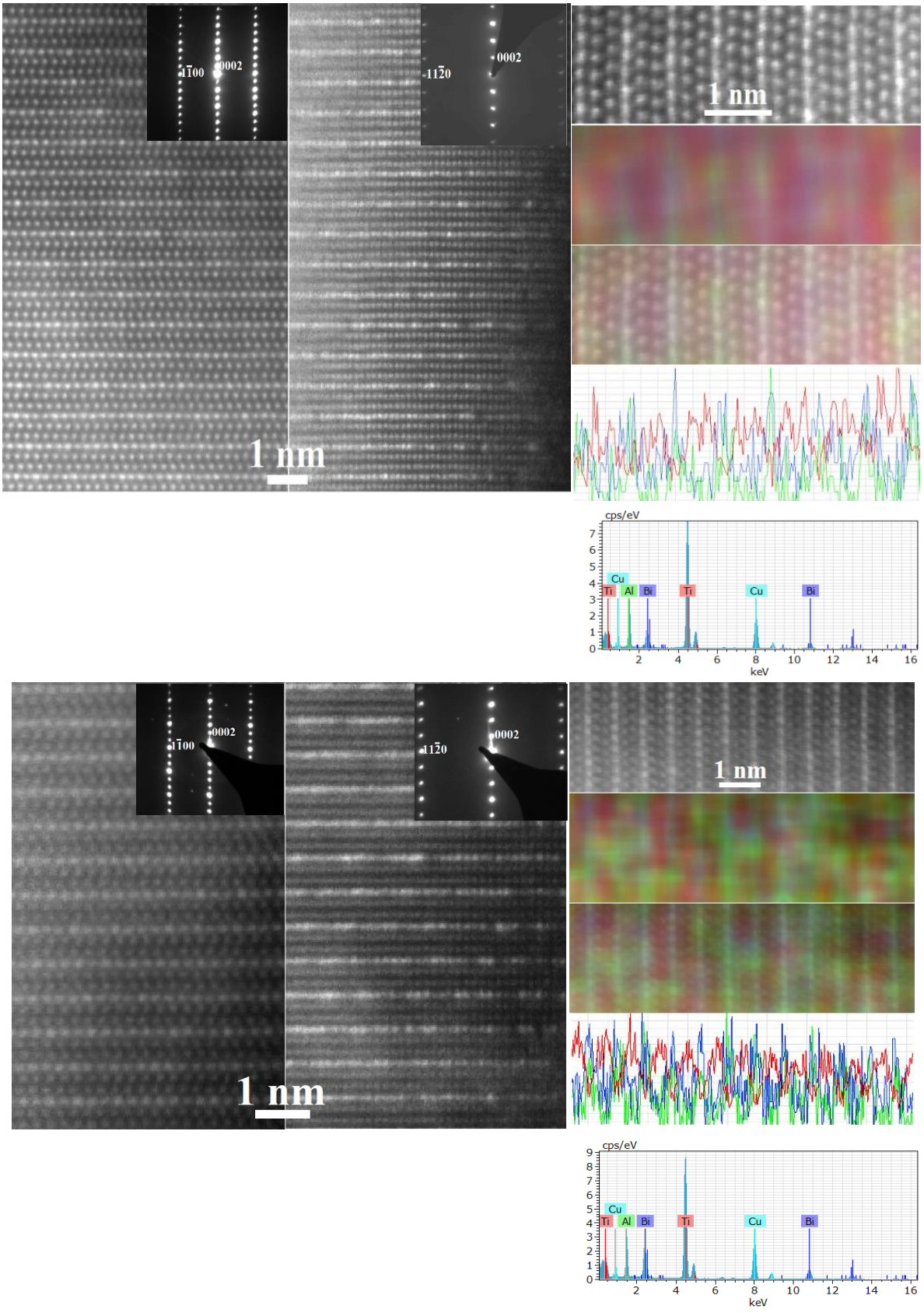

Figure 12. HRSTEM with SAED and EDS results for $Ti_2(Al_{1-x}Bi_x)C$ with targeted x = 0.20 (observed x = 0.17; top) and targeted x = 0.30 (observed x = 0.27; bottom).

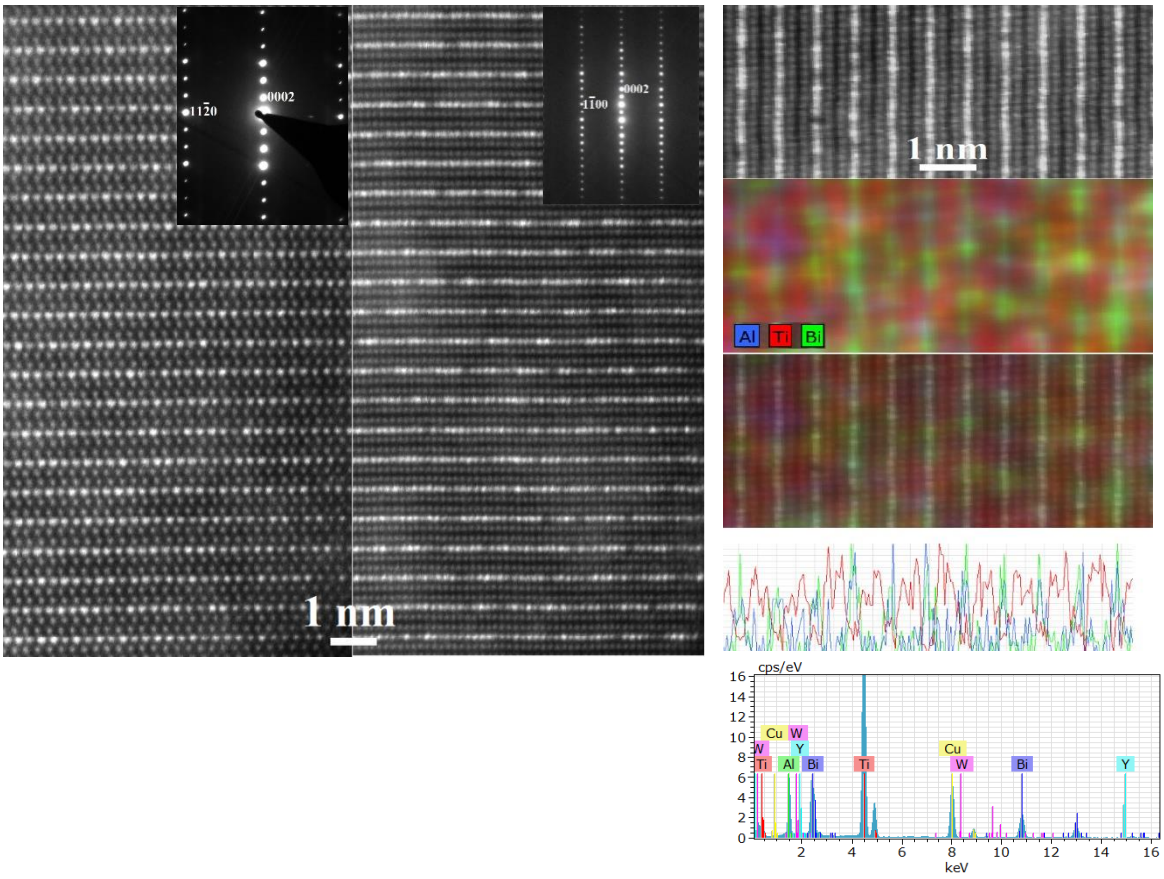

Figure 13. HRSTEM with SAED and EDS results for $Ti_2(Al_{1-x}Bi_x)C$ with targeted x = 0.60 (observed x = 0.31)

To further analyze changes of lattice parameters with increasing amount of Bi in $Ti_2(Al_{1-x}Bi_x)C$, *a* and *c* lattice parameters were determined from XRD results in **Figure 2** and are plotted in **Figure 14** (and summarized in **Table 1**) for $Ti_2(Al_{1-x}Bi_x)C$ samples with different compositions. These results show significant stretching of the crystal structure only in the *a* direction to accommodate larger Bi atom on the A-sublattice, while the *c* lattice parameter remains almost constant with increasing amounts of Bi in $Ti_2(Al_{1-x}Bi_x)C$. Indeed, the computational findings by Chroneos *et. al* also found the gradual increase in the *a* lattice parameter and no changes in the *c* lattice parameter as the amount of bismuth increases in $Zr_2(Al_{1-x}Bi_x)C$ [12]. A similar trend was also observed $Ti_2(Al_{1-x}Sn_x)C$, where increasing amounts of much larger Sn on the A–sublattice also leads to the increase of *a* lattice parameter with no significant change in the *c* lattice

parameter [24]. Therefore, it is reasonable to conclude A element substitution is unlike the substitution of M elements in MAX phase solid solutions, where the crystal lattice expands in both *a* and *c* directions in parallel.

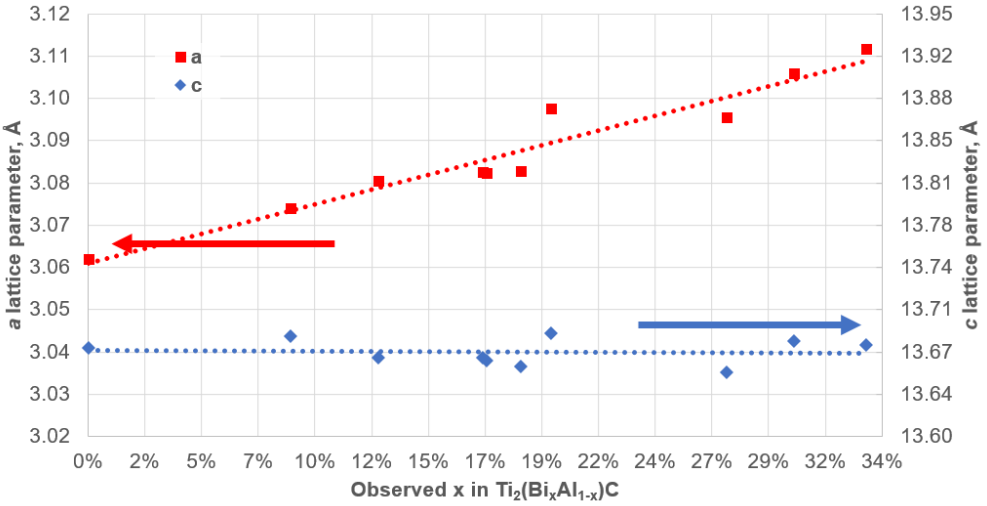

Figure 14. Sampling of* a *and* c *lattice parameters of $Ti_2(Al_{1-x}Bi_x)C$. Data gathered from XRD results in Figure 3 for samples with targeted Bi amount from x = 0.00 to x = 0.80.

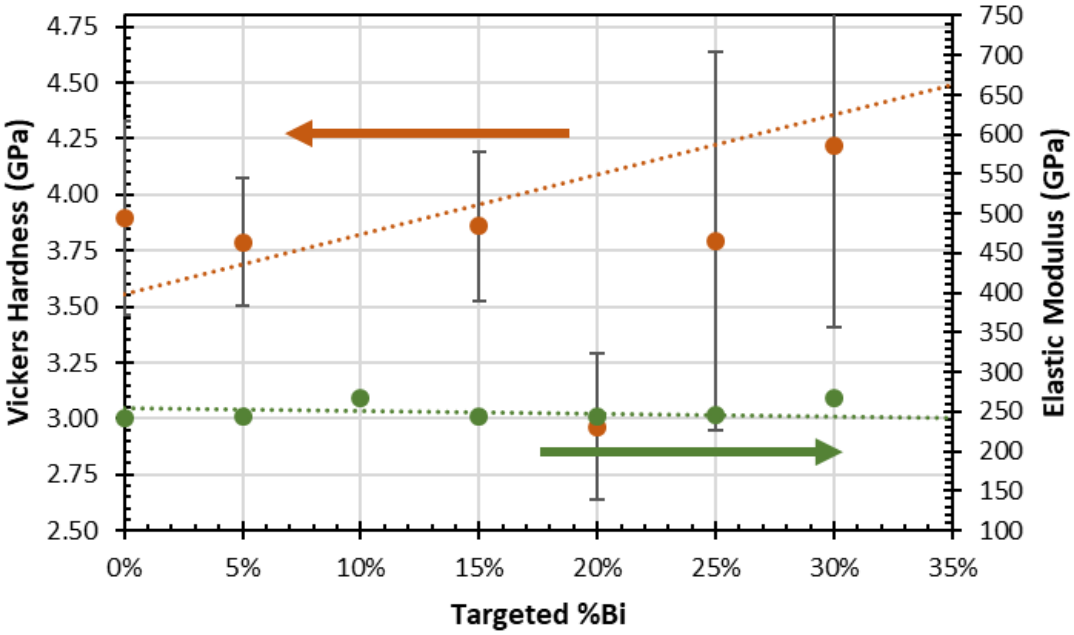

Figure 15. Vickers hardness and Young's modulus of $Ti_2(Al_{1-x}Bi_x)C$ samples with targeted amounts of bismuth ranging from x = 0.00 to x = 0.30.

Vickers hardness measurements were performed for each reaction sintered sample on a minimum of 40 different points for each sample, and the results are summarized in **Figure 15**. As the amount of bismuth in the 211 MAX phase increases, the hardness increases, though not drastically. The standard deviation (indicated by the error bars) is due to local microstructural inhomogeneity. The only exception is the sample with observed composition of $Ti_2(Al_{0.83}Bi_{0.17})_{1.00}C$ that shows slight softening for reasons that are currently unclear.

Resonant Ultrasound Spectroscopy was performed from 50 MHz to 250 MHz with a step size of 5 MHz and a dwell time of 5 μs. Bulk and shear (not pictured) were determined form resonate spectra and results are also summarized in **Figure 15**. None of the aforementioned properties underwent any substantial shift, suggesting a balancing effect between the increased rigidity due to substitution of Al with larger Bi on A-sublattice, and softening caused by imposing more vacancies into the same sublattice. The $Ti_2(Al_{0.62}Bi_{.38})_{0.91}C$ sample was not examined via RUS due to brittle impurities and large amount of microcracks.

Summary of Results

Herein we report for the first time on the synthesis of $Ti_2(Al_{1-x}Bi_x)C$, notable for the large difference in size between A-layer constituents (> 20%). The structure and mechanical properties of all samples were characterized and major findings can be summarized as follows:

- A maximum solubility of Bi in $Ti_2(Al_{1-x}Bi_x)C$ is around 38%, i.e. $x = 0.38$.
- Substitution of Al with Bi in $Ti_2(Al_{1-x}Bi_x)C$ results in the anisotropic stretching of the lattice parameters in the *a* direction, from 3.06 Å to 3.11 Å, with little effect on the *c* lattice parameter.
- The largest number of vacancies on A site ever reported (around 9% of A-sites) forms during synthesis of $Ti_2(Al_{1-x}Bi_x)C$ to accommodate much larger Bi atom on A-sublattice.

Increasing the fraction of bismuth in the $Ti_2(Al_{1-x}Bi_x)C$ phase does not significantly alter hardness or elastic properties, excepting large noise caused by brittle impurities.

CHAPTER III

SYNTHESIS OF $Ti_2(Al_{1-x}Sb_x)C$

Materials and Methods

Titanium, aluminum, antimony and graphite elemental powders (all from Alfa Aesar, MA) were mixed with a Ti:Al:Sb:C stoichiometry of 2 : 1.2(1-x) : 1.15(x) : 0.95. Additional amount of low melting point Al and Sb was added to compensate for their leakage and volatilization during pressure assisted reactions sintering to MAX phase and preferential formation of $TiSb_2$ (see below for more details). Exact mixing ratios of elemental powders for different $Ti_2(Al_xSb_{1-x})C$ solid solutions synthesized in this study are provided in **Table 3**. The powder mixing ratios presented in **Table 3** were selected to maximize the volume fraction of $Ti_2(Al_xSb_{1-x})C$ phase and result from testing many different mixing ratios (not shown here) for each targeted composition. All powder mixtures were ball-milled for 6 hours and compacted into a 20 mm graphite die and reaction sintered using a Pulsed Electric Current Sintering System (Thermal Technologies LLC, CA). Samples were heated to 800°C at a rate of 25°C/min to allow molten antimony to be dissolved into aluminum. After 5 minutes, the pressure on the samples was increased to 15 MPa at a rate of 10 MPa/min and resumed heating at a rate of 25°C/min up to 1400°C. The temperature and pressure were held constant for 15 minutes before rapid cooling and pressure relief.

The surfaces of resulting bulk samples were manually polished and examined using X-Ray diffraction (XRD, D8-Focus Bragg-Brentano X-ray Powder Diffractometer, Bruker) and resulting diffractograms were examined using DIFFRAC.EVA (Bruker) and TOPAS (Bruker) software. Le Bail refinement was performed to determine the lattice parameters of the primary

phases, and Rietveld refinement was used to quantify the phase ratios (by volume) in the bulk. All peak labels and crystal structure information were obtained from the Inorganic Crystal Structure Database (ICSD), and the background was modeled as an amorphous hkl phase. Lattice parameters from Le Bail refinement were further used for Rietveld refinement, and a maximum allowable error threshold was set to $R_{wp} \approx 9.0$.

Table 3. ***Summary of some of the $Ti_2(Al_{1-x}Sb_x)C$ phases synthesized in this study. Included are mixing ratios of initial powders, and results of XRD, SEM and EDS analysis.***

	Mixed		**XRD**		**EDS**					
Target	**Ti : (Al+Sb) : C**	**Al : Sb**	**Lat. Param.**	**Rietveld**	**in 211**	**in 312**	**in area**	**ImageJ**	**M/A Ratio**	**Actual Primary Stoichiometry (assuming C≈1.0)**
x = 0.00	2.0 : 1.15 : 0.95	1.15 : 0.00	*a* = 3.06, *c* = 13.67	**%MAX** = 97.4 with **$TiAl_3$**	-	-	-	**%MAX** = 95.70	2.00	**$Ti_2Al_{1.00}$**
x = 0.10	2.0 : 1.06 : 0.95	0.96 : 0.10	*a* = 3.08, *c* = 13.64	**%MAX** = 97.8 with **$Ti(Sb_mAl_n)$**	x = 0.15	x = 0.14	x = 20.8	**%MAX** = 88.10	2.17	**$Ti_2(Al_{0.85}Sb_{.15})_{0.94}$**
x = 0.20	2.0 : 1.05 : 0.95	0.86 : 0.20	*a* = 3.09, *c* = 13.60	**%MAX** = 93.3 with **$Ti(Sb_mAl_n)$**	x = 0.22	x = 0.19	x = 0.21	**%MAX** = 95.50	2.12	**$Ti_2(Al_{0.78}Sb_{.22})_{0.95}$**
x = 0.30	2.0 : 1.04 : 0.95	0.75 : 0.30	*a* = 3.10, *c* = 13.58	**%MAX** = 94.3 with **$Ti(Sb_mAl_n)$**	x = 0.32	-	x = 0.22	**%MAX** = 93.20	2.00	**$Ti_2(Al_{0.68}Sb_{.32})_{0.96}$**
x = 0.40	2.0 : 1.04 : 0.95	0.64 : 0.40	*a* = 3.11, *c* = 13.57	**%MAX** = 93.2 with **$Ti(Sb_mAl_n)$**	x = 0.41	-	x = 0.21	**%MAX** = 88.80	1.98	**$Ti_2(Al_{0.59}Sb_{.41})_{0.95}$**
x = 0.50	2.0 : 1.04 : 0.95	0.54 : 0.50	*a* = 3.12, *c* = 13.53	**%MAX** = 92.3 with **$Ti(Sb_mAl_n)$**	x = 0.47	-	x = 0.22	**%MAX** = 84.79	1.98	**$Ti_2(Al_{0.53}Sb_{0.47})_{0.97}$**
x = 0.60	2.0 : 1.04 : 0.95	0.44 : 0.60	*a* = 3.13, *c* = 13.53	**%MAX** = 95.1 with **$Ti(Sb_mAl_n)$**	x = 0.56	-	x = 0.19	**%MAX** = 78.50	2.00	**$Ti_2(Al_{0.45}Sb_{.56})_{0.97}$**
x = 0.70	2.0 : 1.09 : 0.95	0.35 : 0.74	*a* = 3.06, *c* = 13.95	**%MAX** = 99.9 with **$Ti(Sb_mAl_n)$**	x = 0.70	x = 0.51	x = 0.16	**%MAX** = 75.20	2.63	**$Ti_2(Al_{0.29}Sb_{.70})_{1.10}$**

After XRD analysis, all samples were cut with a water-cooled low-speed, mounted in epoxy resin (EpoxiCure^{TM} , Buehler), and mechanically polished up to 0.1 µm diamond suspension for Scanning Electron Microcopy (SEM, JEOL 7500). Surface morphology of samples was examined using Everhart-Thornley detector (ETD), while sample phase purity was characterized by a low angle backscatter electron (LABE) detector. Phase composition was estimated from back-scatter electron images using ImageJ software. An energy dispersion X-ray spectroscopy (EDS) detector, which was operated via INCA (Oxford Instruments) software, was used to obtain chemical composition of the primary, 211 MAX phases as well as other impurities presented in the samples. For each sample, a composition was collected using EDS at a minimum of 60 data points.

Results and Discussion

XRD diffractograms collected for all sintered $Ti_2(Al_{1-x}Sb_x)C$ samples are shown in **Figure 16**. Similarly to $Ti_2(Al_{1-x}Bi_x)C$ discussed in the previous chapter, as more antimony with larger atomic radius substitutes Al on the A-sublattice $Ti_2(Al_{1-x}Sb_x)C$, the lattice parameters stretch and result in a corresponding shift of the *hkl* peaks shown in **Figure 16**. To further analyze changes of lattice parameters with increasing amounts of Bi in $Ti_2(Al_{1-x}Sb_x)C$, the *a* and *c* lattice parameters determined form XRD results in **Figure 16** are plotted in **Figure 17** and summarized in **Table 3** for $Ti_2(Al_{1-x}Sb_x)C$ samples with different compositions. Note that the composition of $Ti_2(Al_{1-x}Sb_x)C$ in **Figure 17** is reported as observed composition determined from EDS results, rather than targeted composition for the reasons that are discussed in more detail later in this section. It can be seen in **Figure 17** that, similarly to the case of $Ti_2(Al_{1-x}Bi_x)C$ where the *a*

lattice parameter increases with increasing amount of large Bi atoms on A-sublattice (see **Figure 14**), the *a* lattice parameter of $Ti_2(Al_{1-x}Sb_x)C$ also increases with increasing amounts of large Sb atoms on the A-sublattice. However, while the *c* lattice parameter does not depend on the amount of Bi in A-sublattice in $Ti_2(Al_{1-x}Bi_x)C$ (see **Figure 14**), the *c* lattice parameter in $Ti_2(Al_{1-x}Sb_x)C$ shows some small decrease with increasing amount of large Sb atom on A-sublattice. This difference can be explained by the fact that Sb atom is smaller than that of Bi, so the stretching of MX-trigonal prisms in MAX phase structure in the *a* direction leads to their slight shrinking in the *c* direction, while in the case of substitution with Bi that shrinkage in *c* direction is limited by the larger size of the Bi atom. The other evidence for this can be find in the fact that no significant amount of vacancies on A-sublattice was observed with substitution of large fraction of Al with Sb in $Ti_2(Al_{1-x}Sb_x)C$, unlike in the case of the substitution of Al with much larger Bi in $Ti_2(Al_{1-x}Bi_x)C$, discussed in more detail later. It is therefore reasonable to conclude that the substitution of Al in Ti_2AlC with smaller Sb results in smaller lattice strains than in the case of substitution with larger Bi. As a result , the solubility of Sb in the A-sublattice is much ($x = 0.71$) larger than solubility of Bi ($x = 0.34$), as it can be seen in **Tables 1** and **3**.

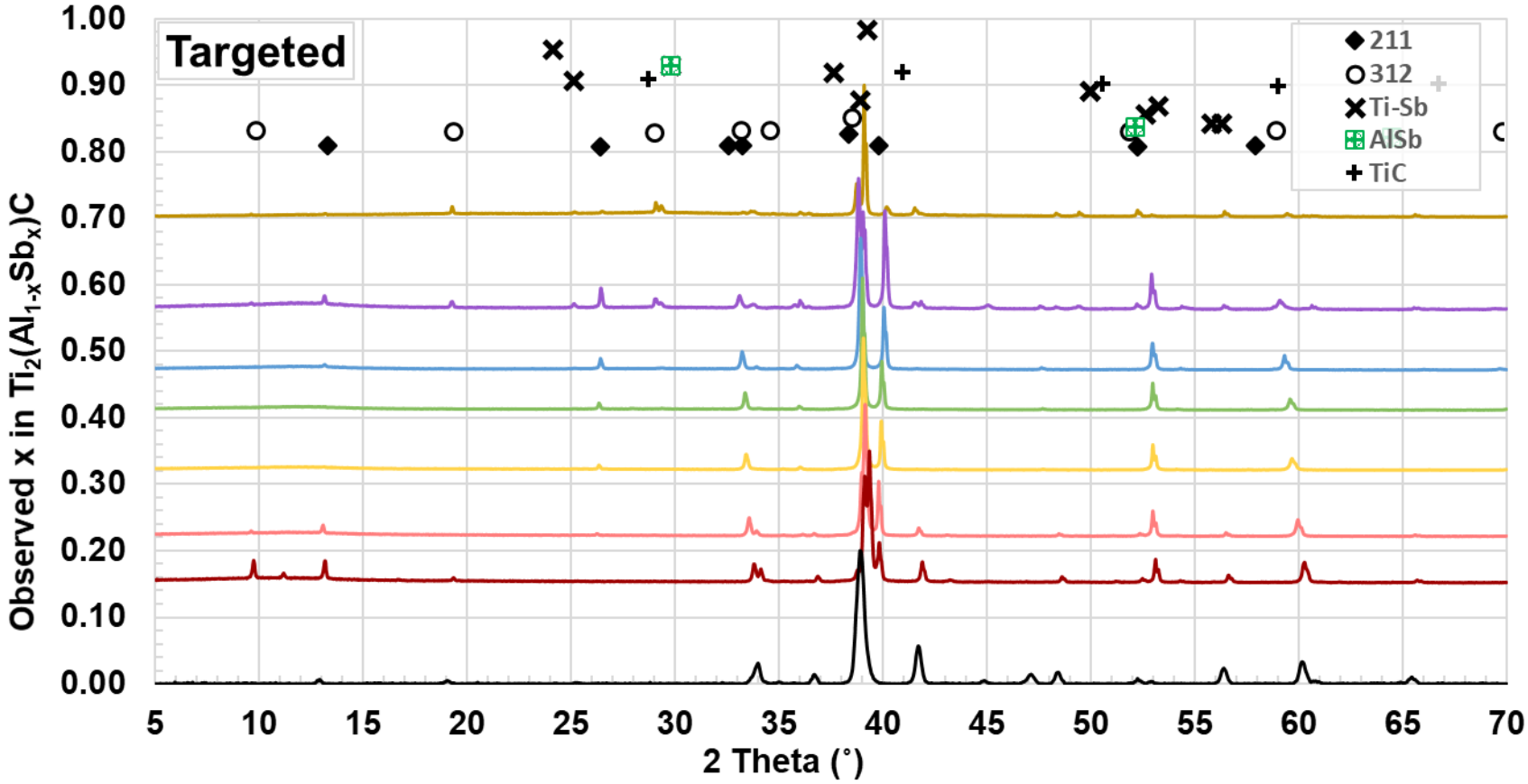

Figure 16. X-ray diffractograms of $Ti_2(Al_{1-x}Sb_x)C$ for observed composition ranging from x = 0.00 to x = 0.70.

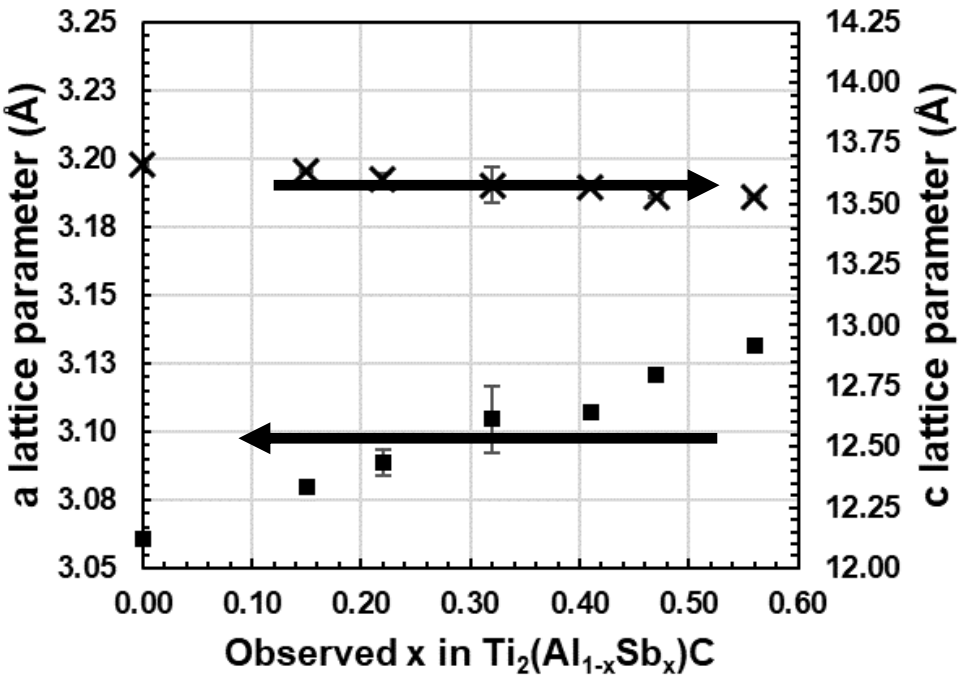

Figure 17. Selected* a *and* c *lattice parameters of $Ti_2(Al_{1-x}Sb_x)C$. Data gathered form XRD results in Figure 16 for samples with targeted Bi amount from x = 0.00 to x = 0.70.

XRD results shown in **Figure 16** also indicate that all sintered samples contain some amount of $Ti_3(Al_{1-x}Sb_x)C_2$ MAX phase along with both TiSb and AlSb intermetallic (excepting $Ti_2(Al_{1-x}Sb_x)C$). However, results of Rietveld analyses depicted in **Table 3** show that the total amount of MAX phases, either $Ti_3(Al_{1-x}Sb_x)C_2$ or $Ti_2(Al_{1-x}Sb_x)C$ is very high, i.e. around 93%, much higher than that observed in most of $Ti_2(Al_{1-x}Bi_x)C$ samples (see **Table 1** and **Figure 18**). Also note that while most impurities are marked in terms of antimony (e.g. Ti_3Sb and $TiSb_2$), the actual intermetallic phases observed in sintered samples contain a large amount of aluminum according to EDS results, shown in **Figure 18**, resulting in a range of XRD peaks shifting.

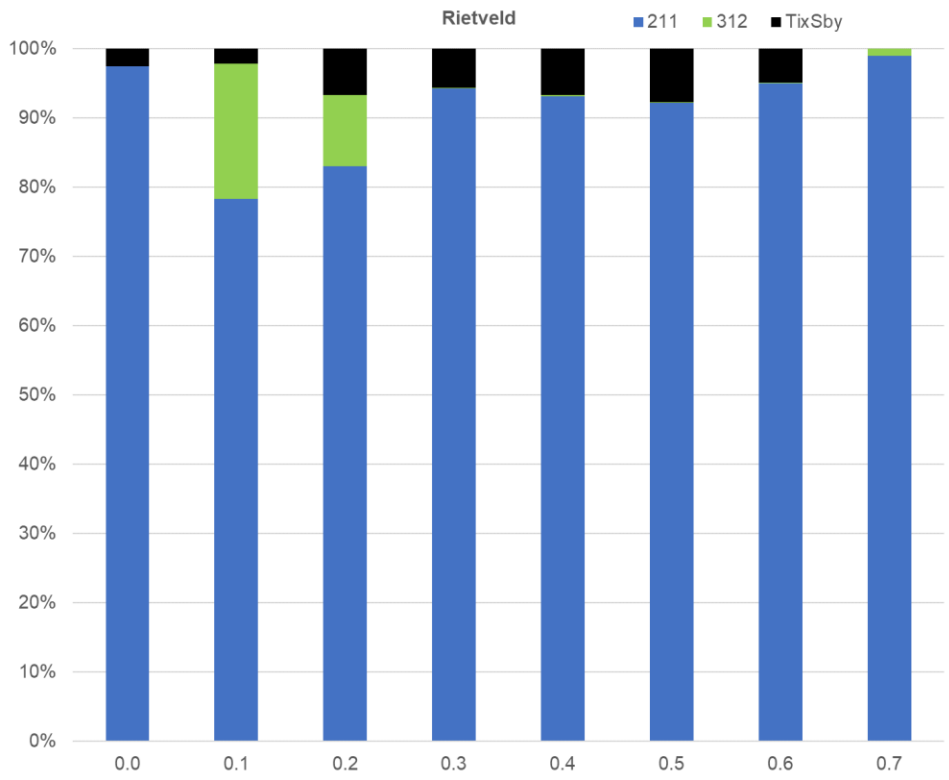

Figure 18. Phase composition by volume percent for $Ti_2(Al_{1-x}Sb_x)C$ with targeted Sb amount ranging from x = 0.00 to x = 0.70 as determined by Rietveld refinement of XRD data.

To better understand the actual amount of antimony incorporated into the $Ti_2(Al_{1-x}Sb_x)C$ phase and to ascertain the stoichiometry of the impurity phases, detailed SEM and EDS analysis was carried out as in the case of $Ti_2(Al_{1-x}Bi_x)C$. Results are summarized in **Figure 19** and **Table 3**. **Figure 19a s**hows select but representative backscattered electron micrographs of each sample with different composition. The darkest spots in those images are lighter intermetallics (mostly $TiAl_3$ and Ti_2Sb in samples with higher targeted x), while the lightest spots are the heavier intermetallics (mostly $TiSb_2$), according to the EDS analysis in those areas (not shown here). The MAX phases show very similar contrast, with $Ti_3(Al_{1-x}Sb_x)C_2$ being slightly darker than $Ti_2(Al_{1-x}Sb_x)C$. **Figure 19b** depicts an EDS map of a selected composition, confirming that Sb is mostly

incorporated in 211 and 312 MAX phases, while smaller amount of Sb primarily TiSb intermetallic impurities.

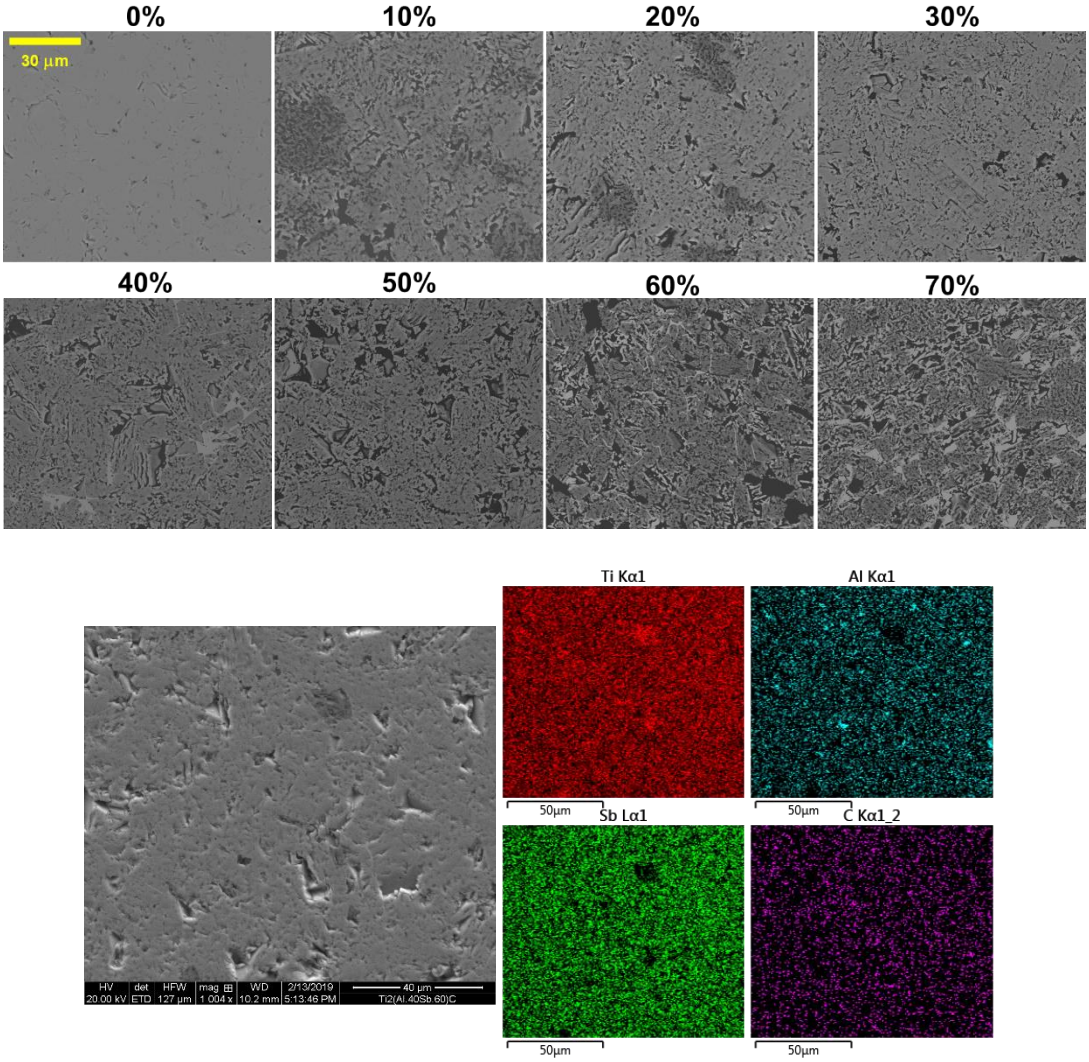

Figure 19. SEM and EDS data of $Ti_2(Al_{1-x}Sb_x)C$. (a) Representative electron backscatter micrographs (equal magnification) of $Ti_2(Al_{1-x}Sb_x)C$ with different targeted amount of Sb, ranging from x = 0.0 to x = 0.7 and (b) EDS map of $Ti_2(Al_{1-x}Sb_x)C$ with targeted x = 0.6 showing antimony preference for substitution in $Ti_2(Al_{1-x}Sb_x)C$ and $Ti_3(Al_{1-x}Sb_x)C_2$ MAX phases (lighter and light gray) followed by Ti_xSb_y intermetallic impurities (very dark and very light spots).

Furthermore, SEM results in **Figures 19** confirm that all reaction sintered samples contain mostly $Ti_2(Al_{1-x}Sb_x)C$ (or 211 phase) and $Ti_3(Al_{1-x}Sb_x)C_2$ (or 312 phase), plus some TiSb impurities that might or might not contain some Al in solid solution. Different phases presented in **Figure 19** were identified based on their chemical composition using EDS (results not shown here). However, phase compositions for $Ti_2(Al_{1-x}Sb_x)C$ samples with different targeted *x* cannot be determined accurately from SEM backscatter electron micrographs using ImageJ, because of the relatively small difference in the phase contrast between $Ti_2(Al_{1-x}Sb_x)C$ and $Ti_3(Al_{1-x}Sb_x)C_2$. Regardless, quantitative EDS analysis was carried out for each sample with different targeted *x* to (i) determine chemical composition of the entire sample by analyzing overall composition of the ~100 x 150 μm representative area, (ii) determine the compositions of major $Ti_2(Al_{1-x}Sb_x)C$ (i.e. 211) phases in at least 10 points. Results of these analyses are summarized in **Table 3**.

These results indicate that the amount of Ti/(Al+Sb) ratio as determined using areal EDS analysis for samples with different targeted Sb amount, *x*, is almost constant, and nearly equal to the stoichiometric ratio of 2. The only exception is the sample with targeted x = 0.7, where this ratio reaches value of 2.63, due to larger amounts of impurities (see **Figure 19a**) that were not reliably detectable by XRD. Most importantly, these results suggest that vacancies do not form in A-sublattice with substitution of Al with Sb, as in the case of substitution of Al with much larger Bi. In addition, unlike in the case of Al substitution with Bi in Ti_2AlC (**Table 1**), the amount of Sb in $Ti_2(Al_{1-x}Sb_x)C$ determined using EDS provided in **Table 3**, is almost identical (within the margin of error) to the targeted amount. The reason for this is that melting point of Sb is 630.1 ^oC, and thus much higher than that one of Bi (274.1 ^oC). Thus smaller amounts of molten Sb are

lost from the powder mixture during reaction sintering due to its leaking from the die and its volatilization. These results show the solubility of Sb on A-sublattice can reach around 70% in Ti_2AlC MAX phase, which is shockingly high considering the instability of Ti_2SbC does not exist. Indeed, attempts to reaction sinter samples with targeted $x > 0.7$ resulted in complete phase decomposition.

Summary of Results

$Ti_2(Al_{1-x}Sb_x)C$ with the notable large difference in size between A-layer elements has been synthesized for the first time. The structure of all samples were characterized and major findings can be summarized as following:

- A maximum solubility of Sb in $Ti_2(Al_{1-x}Sb_x)C$ is around 70%, i.e. $x = 0.70$.
- Substitution of Al with more Sb in $Ti_2(Al_{1-x}Bi_x)C$ results in the stretching of the lattice parameters in the *a* direction and shrinking in the *c* lattice direction.

$Ti_2(Al_{1-x}Sb_x)C$ samples with small amounts of impurities can be reaction sintered with higher Sb content and ease (compared to bismuth substitution into the same phase), due to a smaller amount of molten Sb being lost during reaction sintering.

CHAPTER IV

SUMMARY

Closing Remarks

The major results of this work include:

- The first synthesis of $Ti_2(Al_{1-x}Sb_x)C$ and $Ti_3(Al_{1-x}Sb_x)C_2$, notable for the large difference in size between A-layer constituents, is reported.

- Unlike other large-element-substituted MAX phase solutions, the unit cell tends to remain constant, with an increase 3.06 Å to 3.13 Å in the *a* direction causing a parallel decrease from 13.67 Å to 13.53 Å in the *c* direction.

- Increasing the fraction of antimony in the 211 MAX phase does not significantly alter oxidation resistance.

- Unlike most MAX phase solid solutions, carbides are not the primary impurity, with thermodynamic preference toward antimony-based phases generating large regions of 312 MAX phase.

Conclusions

New MAX phase solid solutions on the A-sublattice, namely $Ti_2(Al_{1-x}Bi_x)C$ and $Ti_2(Al_{1-x}Sb_x)C$, were synthesized for the first time from elemental powders. Results of this study show that MAX phases can be alloyed on A-sublattice using elements that have significantly larger atomic radius and do not form pure MAX phases.

Alloying Ti_2AlC with Bi in the A-sublattice results in the anisotropic stretching of the lattice parameters in the *a* direction, from 3.06 Å to 3.11 Å, with it little effect on the c lattice parameter. In addition, it results in the formation of up to 9% of vacancies on the A site, the largest ever reported vacancy concertation on A site for any MAX phase. Both changes in lattice parameters and the formation of vacancies on the A-sublattice minimize lattice strains caused by substitution of Al with much larger Bi. Results of this study also show that the maximum solubility of Bi in $Ti_2(Al_{1-x}Bi_x)C$ is around 38% (i.e. x = 0.38). Low melting point of Bi, and its leaking and volatilization during reaction sintering is a major challenge for obtained targeted 211 stoichiometry of the sample, it is very difficult to obtain $Ti_2(Al_{1-x}Bi_x)C$ samples with high phase purity with higher Bi content. Interestingly, increasing the fraction of bismuth in the $Ti_2(Al_{1-x}Bi_x)C$ phase does not significantly alter hardness or elastic properties, excepting large noise caused by brittle impurities.

Alloying Ti_2AlC with Sb results not only in the stretching of the lattice parameters in the *a* direction but also shrinkage in the *c* direction, and unlike in the case of alloying with Bi does not form vacancies on the A-sublattice. Results of this study also show that the maximum solubility of Sb in $Ti_2(Al_{1-x}Sb_x)C$ is around 70% (i.e. x = 70), and thus much higher than the maximum

solubility of Bi in $Ti_2(Al_{1-x}Bi_x)C$. $Ti_2(Al_{1-x}Sb_x)C$ samples with only small amounts of impurities can be reaction sintered with high Sb content, due to a smaller amount of molten Sb being lost from the powder mixture during reaction sintering, when compared to Bi due its higher melting point.

The MAX phase alloying space, specifically using multiple A elements, is severely underexplored. This research provides a testament to the unique property of possible tuning of composition, structure and properties of MAX phases by alloying on the A-sublattice, incusing elements that do not form stable end member MAX phases and elements with a substantial difference in atomic radii.

Implications and Future Work

The success in synthesis of these novel predicted MAX phase alloys confirms DFT cluster expansion predictions reported by Arroyave *et al.* [23], thereby encouraging further exploration of the compositional space of MAX phase solid solutions using both computational and experimental approaches. Specifically, lead should exhibit high solubility in both Zr_2AlC and Ti_2AlC and this yet has to be confirmed experimentally. Additionally, the predicted phase separation of Zr_2AlC and Ti_2AlC alloyed with phosphorous, sulfur, and selenium on A-sublattice are both worth exploring experimentally, as such materials would result in two phase MAX phase systems.

Though the M-X bond is clearly the basis for most material properties, one area of research where the M-A bond plays a vital role is in the chemical etching of MAX phases to MXenes. In

this field, weakening the M-A bonds while maintaining the M-X integrity is integral for successful etching to MXene. Incorporation of larger elements (that is, incorporation of elements that also promote vacancy formation) could be the grounds for a dramatic next step in MXenes synthesis form MAX phases. Synthesis of new pristine MXenes, currently impossible to separate the M-A bonds whilst preserving the M-X bonds due to their similarities in energy level, may likely be facilitated by A-alloying or distortion-induced vacancies.

REFERENCES

1. Radovic M, Barsoum MW. MAX phases: bridging the gap between metals and ceramics. American Ceramics Society Bulletin. 2013;92:20-7.
2. Barsoum MW, Radovic M. Elastic and mechanical properties of the MAX phases. Annual review of materials research. 2011;41:195-227.
3. Barsoum MW. MAX phases: properties of machinable ternary carbides and nitrides: John Wiley & Sons; 2013.
4. Sokol, M., Natu, V., Kota, S. and Barsoum, M.W., 2019. On the chemical diversity of the MAX phases. Trends in Chemistry.
5. Jeitschko W, Nowotny H, Benesovsky F. Ti 2 AlN, eine stickstoffhaltige H-phase. Monatshefte für Chemie/Chemical Monthly. 1963;94:1198-200.
6. Schuster J, Nowotny H, Vaccaro C. The ternary systems: CrAlC, VAlC, and TiAlC and the behavior of H-phases (M2AlC). Journal of Solid State Chemistry. 1980;32:213-9.
7. Barsoum MW, El-Raghy T. Synthesis and characterization of a remarkable ceramic: Ti3SiC2. Journal of the American Ceramic Society. 1996;79:1953-6.
8. Basu S, Obando N, Gowdy A, Karaman I, Radovic M. Long-term oxidation of Ti2AlC in air and water vapor at 1000–1300 C temperature range. Journal of the Electrochemical Society. 2011;159:C90-C6.
9. Tallman DJ, Anasori B, Barsoum MW. A critical review of the oxidation of Ti2AlC, Ti3AlC2 and Cr2AlC in air. Materials Research Letters. 2013;1:115-25.
10. Wang X, Zhou Y. Layered machinable and electrically conductive Ti (2) AlC and Ti (3) AlC (2) ceramics: a review. 2010.

11. Horlait D, Grasso S, Chroneos A, Lee WE. Attempts to synthesise quaternary MAX phases (Zr, M) 2AlC and Zr2 (Al, A) C as a way to approach Zr2AlC. Materials Research Letters. 2016;4:137-44.

12. Lin S, Huang Y, Zu L, Kan X, Lin J, Song W, Tong P, Zhu X, Sun Y. Alloying effects on structural, magnetic, and electrical/thermal transport properties in MAX-phase Cr2− xMxGeC (M= Ti, V, Mn, Fe, and Mo). Journal of Alloys and Compounds. 2016;680:452-61.

13. Horlait D, Middleburgh SC, Chroneos A, Lee WE. Synthesis and DFT investigation of new bismuth-containing MAX phases. Scientific reports. 2016;6:18829.

14. Liu Z, Wu E, Wang J, Qian Y, Xiang H, Li X, Jin Q, Sun G, Chen X, Wang J. Crystal structure and formation mechanism of (Cr2/3Ti1/3) 3AlC2 MAX phase. Acta Materialia. 2014;73:186-93.

15. Anasori B, Dahlqvist M, Halim J, Moon EJ, Lu J, Hosler BC, Caspi EaN, May SJ, Hultman L, Eklund P. Experimental and theoretical characterization of ordered MAX phases Mo2TiAlC2 and Mo2Ti2AlC3. Journal of Applied Physics. 2015;118:094304.

16. Meshkian R, Tao Q, Dahlqvist M, Lu J, Hultman L, Rosen J. Theoretical stability and materials synthesis of a chemically ordered MAX phase, Mo2ScAlC2, and its two-dimensional derivate Mo2ScC2 MXene. Acta Materialia. 2017;125:476-80.

17. Dahlqvist M, Lu J, Meshkian R, Tao Q, Hultman L, Rosen J. Prediction and synthesis of a family of atomic laminate phases with Kagomé-like and in-plane chemical ordering. Science advances. 2017;3:e1700642.

18. Naguib M, Mochalin VN, Barsoum MW, Gogotsi Y. 25th anniversary article: MXenes: a new family of two-dimensional materials. Advanced Materials. 2014;26:992-1005.

19. Tao Q, Dahlqvist M, Lu J, Kota S, Meshkian R, Halim J, Palisaitis J, Hultman L, Barsoum MW, Persson PO. Two-dimensional Mo 1.33 C MXene with divacancy ordering prepared from parent 3D laminate with in-plane chemical ordering. Nature communications. 2017;8:14949.

20. Ashton M, Hennig RG, Broderick SR, Rajan K, Sinnott SB. Computational discovery of stable M 2 A X phases. Physical Review B. 2016;94:054116.

21. Hamm CM, Dürrschnabel M, Molina-Luna L, Salikhov R, Spoddig D, Farle M, Wiedwald U, Birkel CS. Structural, magnetic and electrical transport properties of non-conventionally prepared MAX phases V 2 AlC and (V/Mn) 2 AlC. Materials Chemistry Frontiers. 2018;2:483-90.

22. Yeh C, Chen J. Combustion synthesis of Ti3Si1− xAlxC2 solid solutions from TiC-, SiC-, and Al4C3-containing powder compacts. Journal of Alloys and Compounds. 2011;509:7277-82.

23. Petruhins, Andrejs, Jun Lu, Lars Hultman, and Johanna Rosen. "Synthesis of atomically layered and chemically ordered rare-earth (RE) i-MAX phases;(Mo2/3RE1/3) 2GaC with RE= Gd, Tb, Dy, Ho, Er, Tm, Yb, and Lu." Materials Research Letters 7, no. 11 (2019): 446-452.

24. Etzkorn J, Ade M, Kotzott D, Kleczek M, Hillebrecht H. Ti 2 GaC, Ti 4 GaC 3 and Cr 2 GaC—Synthesis, crystal growth and structure analysis of Ga-containing MAX-phases Mn+ 1 GaCn with M= Ti, Cr and n= 1, 3. Journal of Solid State Chemistry. 2009;182:995-1002.

25. Lapauw T, Lambrinou K, Cabioc'h T, Halim J, Lu J, Pesach A, Rivin O, Ozeri O, Caspi E, Hultman L. Synthesis of the new MAX phase Zr2AlC. Journal of the European Ceramic Society. 2016;36:1847-53.

26. Arróyave R, Talapatra A, Duong T, Son W, Gao H, Radovic M. Does aluminum play well with others? Intrinsic Al-A alloying behavior in 211/312 MAX phases. Materials Research Letters. 2017;5:170-8.

27. Bei G, Pedimonte BJ, Fey T, Greil P. Oxidation behavior of MAX phase Ti 2 Al (1− x) Sn x C solid solution. Journal of the American Ceramic Society. 2013;96:1359-62.

28. Yeh C, Chiang C. Combustion synthesis of Ti2 (Al, Sn) C solid solutions from Ti/Al/Sn/C samples with addition of TiC and Al4C3. Ceramics International. 2015;41:6263-8.

29. Cai L, Huang Z, Hu W, Hao S, Zhai H, Zhou Y. Fabrication, mechanical properties, and tribological behaviors of Ti2AlC and Ti2AlSn0. 2C solid solutions. Journal of Advanced Ceramics. 2017;6:90-9.

30. Bortolozo A, Sant'Anna O, Dos Santos C, Machado A. Superconductivity at 9.5 K in the Ti 2 GeC compound. Materials Science-Poland. 2012;30:92-7.

31. Jeitschko W, Nowotny H, Benesovsky F. Die H-Phasen Ti 2 TlC, Ti 2 PbC, Nb 2 InC, Nb 2 SnC und Ta 2 GaC. Monatshefte für Chemie und verwandte Teile anderer Wissenschaften. 1964;95:431-5.

32. Zhou Y, Dong H, Wang X, Yan C. Preparation of Ti2SnC by solid—liquid reaction synthesis and simultaneous densification method. Materials Research Innovations. 2002;6:219-25.

33. Hadi M, Vovk R, Chroneos A. Physical properties of the recently discovered Zr2 (Al1−xBix) C MAX phases. Journal of Materials Science: Materials in Electronics. 2016;27:11925-33.

34. Radovic, Miladin, M. W. Barsoum, A. Ganguly, T. Zhen, P. Finkel, S. R. Kalidindi, and Edgar Lara-Curzio. "On the elastic properties and mechanical damping of Ti3SiC2, Ti3GeC2, Ti3Si0. 5Al0. 5C2 and Ti2AlC in the 300–1573 K temperature range." Acta Materialia 54, no. 10 (2006): 2757-2767.

35. Radovic, M., Lara-Curzio, E. and Riester, L., 2004. Comparison of different experimental techniques for determination of elastic properties of solids. Materials Science and Engineering: A, 368(1-2), pp.56-70.

36. Radovic, M., Lara-Curzio, E., Trejo, R.M., Wang, H. and Porter, W.D., 2009. Thermophysical properties of YSZ and Ni-YSZ as a function of temperature and porosity. Advances in Solid Oxide Fuel Cells II: Ceramic Engineering and Science Proceedings, Cocoa Beach, 27(4), p.79.

37. Pham, H.H., Williams, M.E., Mahaffey, P., Radovic, M., Arroyave, R. and Cagin, T., 2011. Finite-temperature elasticity of fcc Al: Atomistic simulations and ultrasonic measurements. Physical Review B, 84(6), p.064101.

38. E. Prehn, Z. Tan, T. Duong, J. Lu, J. Rosen, R. Arroyave, M. Radovic, “Synthesis, structure, and mechanical properties of Ti2(Al,Bi)C”, in preparation (2019).

APPENDIX

NOMENCLATURE

MAX	Atomically ordered composite with structure $M_{n+1}AX_n$, where M is a transition metal, A is a late or post-transition metal, and X is carbon or nitrogen. 211 refers to n = 1, 312 refers to n = 2.
MXene	Atomically layered carbide/nitride, typically formed by harsh chemical etching of the A layer in a MAX phase.
EDS/EDX	Electron Dispersion X-Ray Spectroscopy
HR-STEM	High Resolution Scanning Transmission Electron Microscopy
RUS	Resonant Ultrasound Spectroscopy
SAED	Selected Area Electron Diffraction
SEM	Scanning electron microscopy
TEM	Transmission Electron Microscopy
XRD	X-Ray Diffraction